

**A Computational Study of Direct Thermocatalytic Reduction of CO<sub>2</sub> for  
the Production of Synthetic Methanol**

BY

**ILARIA TAGLIAFERRI**

B.S., Politecnico di Torino, Turin, Italy, 2019

THESIS

Submitted as partial fulfillment of the requirements  
for the degree of Master of Science in Energy and Nuclear Engineering  
in the Graduate College of  
Politecnico di Torino , 2021

Torino, Italy

Massimo Santarelli, Advisor at Politecnico di Torino

Suresh Aggarwal, Advisor at University of Illinois at Chicago

## ACKNOWLEDGMENTS

I would like to acknowledge and thank my advisors Professor Suresh Aggarwal and Professor Massimo Santarelli, who gave me the opportunity to work on this project. I would also thank my committee members, Professor Suresh Aggarwal, Professor Massimo Santarelli and Doctor Partick Lynch, for listening to my defense and supporting my work. Thank you also to Jenna Stephens, for making this year a little bit easier with your help and motherly friendship.

The biggest thanks are to my mother and father, they gave me the strength of finish my work and supported financially in all my studies. They have always believed in everything I've done and I could have never asked for more. Next, I would like to thank my brother, who bitter love forged me in the competitive and determined person I am today.

I also would like to acknowledge all the friends that accompanied me from high school to here, they have been close even when I was far. I moved many times but with them, my heart is always at home. A special mention to Giulia, who is my opposite and, literally, my better half.

I would like to thank all the guys who made this experience in Chicago amazing; in particular Matteo, who cheered me up whenever I was in need and always stood by my side.

Finally, I would like to thank the Politecnico di Torino, there I met some of the greatest people I have ever had the pleasure to encounter and it gave me the opportunity to grow as a student and, most importantly, as a person.

## TABLE OF CONTENTS

<b><u>CHAPTER</u></b>		<b><u>PAGE</u></b>
<b>1</b>	<b>INTRODUCTION . . . . .</b>	<b>1</b>
<b>2</b>	<b>PRODUCTION OF METHANOL . . . . .</b>	<b>16</b>
2.0.1	Possible Sources of CO <sub>2</sub> . . . . .	17
2.1	Carbon Capture Technologies . . . . .	19
2.1.1	Comparison between Pure MEA and Ionic Liquids Blend . . . . .	23
2.2	Electrolyzer . . . . .	24
2.2.1	Source of Electricity . . . . .	29
2.2.2	Intermittent Electrolyzer Working Conditions . . . . .	30
2.3	Reactor . . . . .	31
2.4	Methanol separation . . . . .	33
<b>3</b>	<b>CATALYST CHARACTERIZATION AND KINETIC MODEL . . . . .</b>	<b>35</b>
3.1	Kinetic Model . . . . .	37
<b>4</b>	<b>MATHEMATICAL MODEL . . . . .</b>	<b>41</b>
4.1	Geometry Simplification . . . . .	42
4.2	Model of the One-Dimensional Pseudo-Homogeneous Fixed-Bed Reactor . . . . .	43
4.2.1	Boundary Conditions: 1D Model . . . . .	51
4.2.2	Computational Model: 1D Model . . . . .	52
4.2.3	Results and Validation: 1D Model . . . . .	55
4.3	Two-Dimensional, Pseudo-Homogeneous Reactor Model . . . . .	65
4.3.1	Boundary Conditions: 2D Model . . . . .	66
4.3.2	2D Computational model . . . . .	67
4.4	Results and Comparison between 1D and 2D model . . . . .	68
<b>5</b>	<b>THERMAL INTEGRATION . . . . .</b>	<b>76</b>
5.1	Pinch Analysis . . . . .	77
5.2	Main Thermal Streams in the Process . . . . .	78
5.3	Design of the Heat Exchangers' Network . . . . .	94
<b>6</b>	<b>CONCLUSIONS . . . . .</b>	<b>100</b>
	<b>CITED LITERATURE . . . . .</b>	<b>102</b>
	<b>VITA . . . . .</b>	<b>107</b>

## LIST OF TABLES

<u>TABLE</u>		<u>PAGE</u>
I	COMPARISON BETWEEN PURE MEA AND BLEND [Bpy][BF <sub>4</sub> ]	24
II	TECHNOLOGIES TO PRODUCE RENEWABLE ELECTRICITY	30
III	CHARACTERISTIC OF CuO/ZnO/Al <sub>2</sub> O <sub>3</sub> CATALYST . . . . .	37
IV	KINETIC PARAMETERS OF THE REACTIONS . . . . .	39
V	PARAMETERS OF EQ. (4.1) TO EQ. (4.4) . . . . .	45
VI	PARAMETERS OF DYNAMIC VISCOSITY . . . . .	46
VII	VALUES OF b OBTAINED BY GARG AND ACHARI [38] . . .	47
VIII	PARAMETERS OF THE MASS BALANCE EQUATION . . . .	49
IX	SHELL AND TUBE REACTOR CHARACTERISTICS . . . . .	58
X	OPTIMAL CONDITIONS FOR METHANOL PRODUCTION .	73
XI	NET CO <sub>2</sub> AND H <sub>2</sub> NEEDS . . . . .	79
XII	ENERGY NEEDS FOR STRIPPING . . . . .	80
XIII	CHARACTERISTIC OF THE CO <sub>2</sub> COMPRESSOR . . . . .	80
XIV	ENERGY NEEDS FOR THE COMPRESSION OF CO <sub>2</sub> . . . . .	81
XV	CHARACTERISTIC OF THE H <sub>2</sub> COMPRESSOR . . . . .	82
XVI	ENERGY NEEDS FOR THE COMPRESSION OF H <sub>2</sub> . . . . .	82
XVII	ENERGY EXTRACTED FROM THE REACTORS . . . . .	83
XVIII	ENERGY SUBTRACTED FROM THE PRODUCTS . . . . .	84
XIX	COMPRESSORS FOR THE RECIRCULATED GASES . . . . .	84
XX	ENERGY NEEDS FOR COMPRESSION OF RECIRC. GASES	85
XXI	MAIN THERMAL STREAMS . . . . .	86
XXII	COLD COMPOSITE CURVE . . . . .	87
XXIII	HOT COMPOSITE CURVE . . . . .	87
XXIV	THERMAL LOADS AND INTEGRATION - PURE MEA PLANT	90
XXV	INTEGRATION FOR DIFFERENT ΔT - PURE MEA PLANT	91
XXVI	THERMAL INTEGRATION - ILB PLANT . . . . .	93
XXVII	THERMAL STREAMS - PURE MEA PLANT . . . . .	94
XXVIII	PINCH POINT ANALYSIS - PURE MEA PLANT . . . . .	96
XXIX	HEAT EXCHANGERS' NETWORK - PURE MEA CASE . . . .	98
XXX	PARAMETERS FOR THE COST OF HEAT EXCHANGERS . .	99

## LIST OF FIGURES

<u>FIGURE</u>		<u>PAGE</u>
1	Global energy TFC by sector in year 2018 . . . . .	1
2	Anthropogenic $CO_2$ emission for possible WGIII scenarios . . . . .	2
3	How cumulative $CO_2$ emissions will probably effect temperature change	2
4	Change in energy consumption and renewable output in 2019-2020 .	4
5	Increase in the production of biofuels in the U.S. vs price of crude .	5
6	Energy consumption and renewable share in transport sector in 2018	6
7	Electricity withdraw from the grid: sunny vs cloudy day comparison	7
8	Possible uses of captured carbon dioxide [9] . . . . .	9
9	Global methanol application and transformation in 2016 . . . . .	11
10	Simplified scheme for methanol synthesis from syngas [15] . . . . .	13
11	Schematic process for production of $CH_3OH$ from $CO_2$ rich stream .	17
12	Working principle of a membrane CC technology [23] . . . . .	20
13	Scheme of the process of $CO_2$ capture by absorption . . . . .	21
14	Schematic of an Alkaline Electrolyzer [26] . . . . .	26
15	PEM electrolyzer principle [27] . . . . .	27
16	Solid Oxide electrolyzer principle [28] . . . . .	28
17	Schematic of a shell-and-tubes reactor . . . . .	33
18	Schematic of the separation columns . . . . .	34
19	General scheme of a shell and tubes reactor [35] . . . . .	43
20	Effect of mesh refinement on outlet mixture composition - 1D . . . .	55
21	Model validation: reacted $CO_2$ . . . . .	57
22	Model validation: methanol yield . . . . .	57
23	Outlet composition dependence on the inlet composition . . . . .	59
24	Methanol yield and selectivity dependence on the inlet composition	60
25	Outlet stream composition dependence on the inlet pressure . . . . .	61
26	Methanol yield and selectivity dependence on the inlet pressure . . .	62
27	Outlet stream composition dependence on the inlet temperature . . .	63
28	Methanol yield and selectivity dependence on the inlet temperature	64
29	How the mesh refinement affects the result - 2D model . . . . .	68
30	Velocity field . . . . .	69
31	Temperature field . . . . .	69
32	$CH_3OH$ and $CO$ molar ratio at the axis and the outer boundary . .	70
33	1D vs 2D dependence on the inlet composition . . . . .	71
34	1D vs 2D dependence on the inlet pressure . . . . .	71
35	1D vs 2D dependence on the inlet temperature . . . . .	72
36	Concentration of the species along the axis of the reactor . . . . .	74
37	Temperature along the axis of the reactor . . . . .	74
38	Temperature along the axis of the reactor with doubled inlet flow .	75

## LIST OF FIGURES (continued)

<u>FIGURE</u>		<u>PAGE</u>
39	Composite curves thermal integration - case of pure MEA . . . . .	88
40	Composite curves thermal integration - $\Delta T=10$ K . . . . .	89
41	Composite curves thermal integration - ILB plant, $\Delta T=10$ K . . . . .	92
42	Composite curves thermal integration - ILB plant, $\Delta T=89$ K . . . . .	92
43	Heat exchangers' network . . . . .	97

## LIST OF ABBREVIATIONS

UIC	University of Illinois at Chicago
GHGs	Green House Gasses
TFC	Total Final Consumption
IPCC	Intergovernmental Panel on Climate Change
AR5	IPCC Fifth Assessment Report
WGIII	Working Group III-IPCC
SUV	Sport Utility Vehicle
CCS	Carbon Capture and Storage
CCU	Carbon Capture and Utilization
DME	Dimethyl Ether
MEA	monoethanolamine
DAC	Direct Atmosphere Capture of the CO <sub>2</sub>
MOFs	Metal-Organic Frameworks materials
EOR	Enhanced Oil Recovery
EGR	Enhanced Gas Recovery
ECBM	Enhanced coal bed methane recovery
FT	Fisher Tropsch

## LIST OF ABBREVIATIONS (continued)

CTL	coal-to-liquids
GTL	gas-to-liquids
PPM	Parts Per Million
FEM	Finite Element Method

## SUMMARY

Methanol can be used as a starting component for the chemical and pharmaceutical industry, as well as a transport fuel in already existing engines.

Currently, methanol is mostly produced from syngas, which, in turn, is obtained from fossil fuels. This aspect makes it a not-suitable solution to target the environmental goals proposed by many governments. However, a sustainable alternative exists: methanol can be produced through the direct thermocatalytic conversion of carbon dioxide.

The aim of this study is to develop 1D and 2D axisymmetric models of a reactor used to convert  $\text{CO}_2$  and  $\text{H}_2$  into  $\text{CH}_3\text{OH}$ . The models have been validated with data obtained in literature. Then, the effects of the inlet pressure, temperature and composition on the reactor performance have been assessed.

Using the computed optimum values of 5 MPa, 240 °C and 3  $\text{H}_2:\text{CO}_2$ , the selectivity of the catalyst used is 81.4 % and the methanol yield is 30.1 %. In addition, from the simulation, the amount of heat that can be extracted from the reactor, in order to control the temperature in the reactor, is obtained. With this value, a thermal integration of the overall plant is studied, and a schematic heat exchangers' network is proposed.

Finally, a plant that uses pure monoethylamine as solvent for carbon capture has been compared with one that uses a blending of ionic liquid and monoethylamine. The second alternative allows us to reduce the heat needed in the system; however, the cost of capturing  $\text{CO}_2$  is higher. For

## SUMMARY (continued)

this reason, a thermo-economic study of the overall plant should be performed in order to determine which solution would maximize the economic return on investment.

## CHAPTER 1

### INTRODUCTION

The expected rise in world's population (from 7 to 9 billion by 2050) along with the living standards are the main driving forces for the increase in global energy demand. As indicated in Fig. 1, the two most energy intensive sectors are industry and transport, which account for almost 60 % of the total energy consumption, and are also the major sources of GHGs emissions.

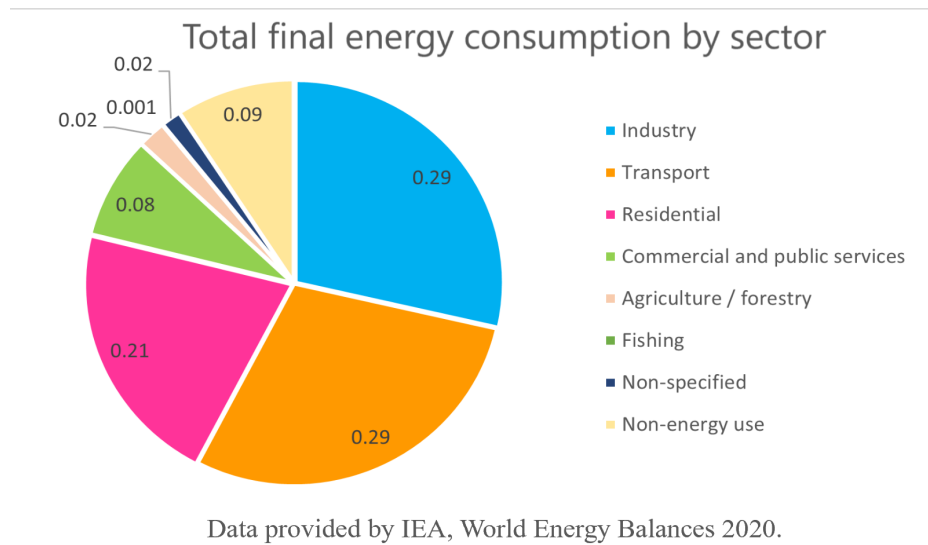
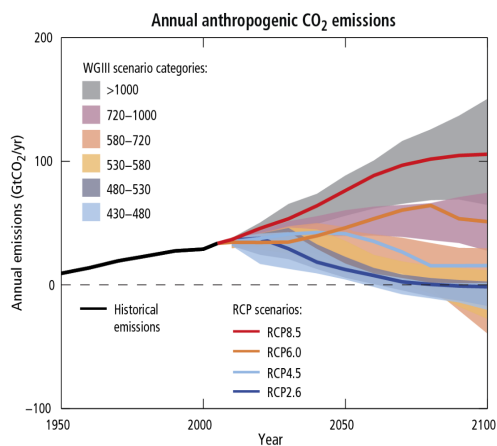


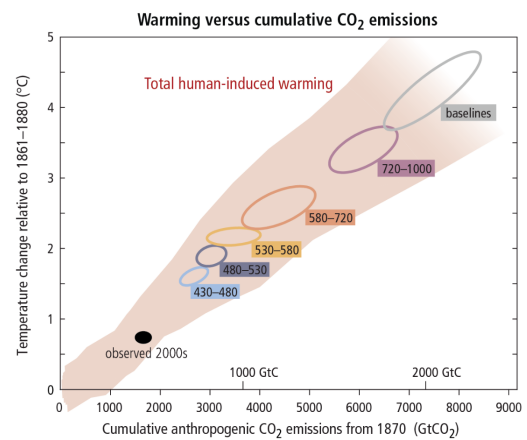
Figure 1: Global energy TFC by sector in year 2018

It has been clearly established by scientists that there is a strong link between CO<sub>2</sub> emissions and increase in the temperature of Earth [1], because of the unbalance caused by CO<sub>2</sub> along with other gases and particulates on the natural Green House effect. Moreover, the amount of anthropogenic GHGs produced and released into the atmosphere continue to increase each year, which could lead to catastrophic events. It is therefore essential to reduce GHG emissions and transition towards a more sustainable path. AR5 synthesis report showed different possible GHG emission pathways [2], indicating that zero net emission, and possibly negative emission, pathway would be needed to meet the target of not exceeding the 2 °C temperature increase since pre-industrial era.



Adapted [reprinted] from \textbf{IPCC}, 2015: AR5 Synthesis Report: Climate Change 2014, IPCC Report Graphics SMP.05-01

Figure 2: Anthropogenic CO<sub>2</sub> emission for possible WGIII scenarios



Adapted [reprinted] from \textbf{IPCC}, 2015: AR5 Synthesis Report: Climate Change 2014, IPCC Report Graphics SMP.05-01

Figure 3: How cumulative CO<sub>2</sub> emissions will probably effect temperature change

Due to the Covid-19 pandemic, energy demand fell dramatically in 2020, followed by the highest percentage decrease in emissions ever recorded of -7% compared to year 2019. The decrease was common to all sectors except for emissions from SUVs [3], which was due to their lower fuel efficiency and higher in sale. Nevertheless, the transportation sector may be the most difficult to make a transition toward an environmentally sustainable direction, in spite of significant efforts over many years to develop alternative fuels. This is due to the need to fulfill many constraints that this sector requires, in terms of size of the engines, technology and infrastructure.

In the Renewable Energy Directive II, there is significant focus on the production of fuels from alternative sources, with the objective of supplying at least 14% of fuel from renewable sources for road and rail transport in the European Union by 2030 [4]. However, due to the lower economic activity in the year 2020 there was a decrease in renewable fuel output. Therefore, to achieve the target the Directive set by 2030, more efforts should be focused in producing such fuels. For this reason, many technologies built to produce fuels from biomass have been investigated and optimized in the past years, bringing back attention on biofuels. The ones derived from biomass or bio waste are the first- and second-generation biofuels and they have been studied since the first years of twentieth century. For example, Rudolf Diesel invented his engine to run on peanut oil, while Henry Ford designed his model T car to work only on fuels derived from hemp [5]. Because of the exploration and production of abundant quantity of crude oil, the cost of petrol decreased. This led engineers to abandon biofuels in favor of the

cheaper alternative.

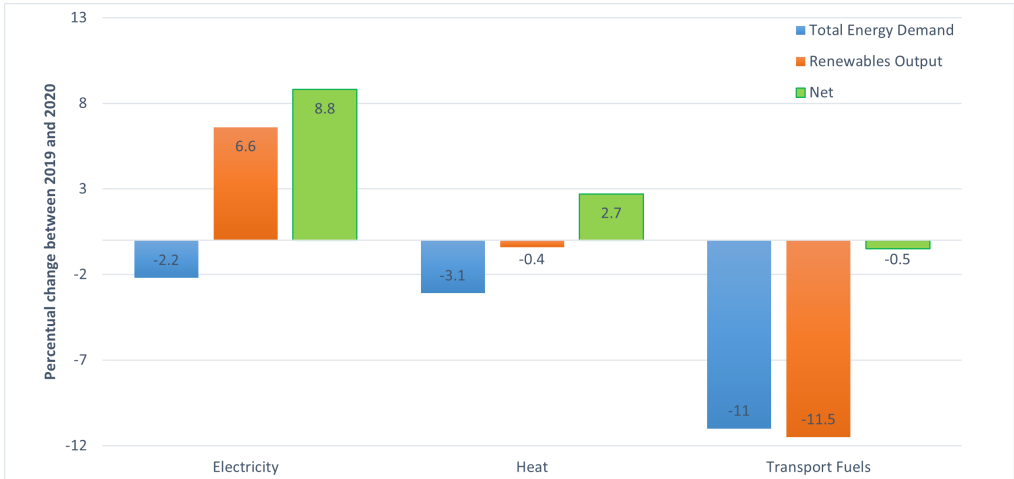


Figure 4: Change in energy consumption and renewable output in 2019-2020

However, with the petroleum crisis, a new interest about alternative fuels rose, generating a new market specially in North and South America.

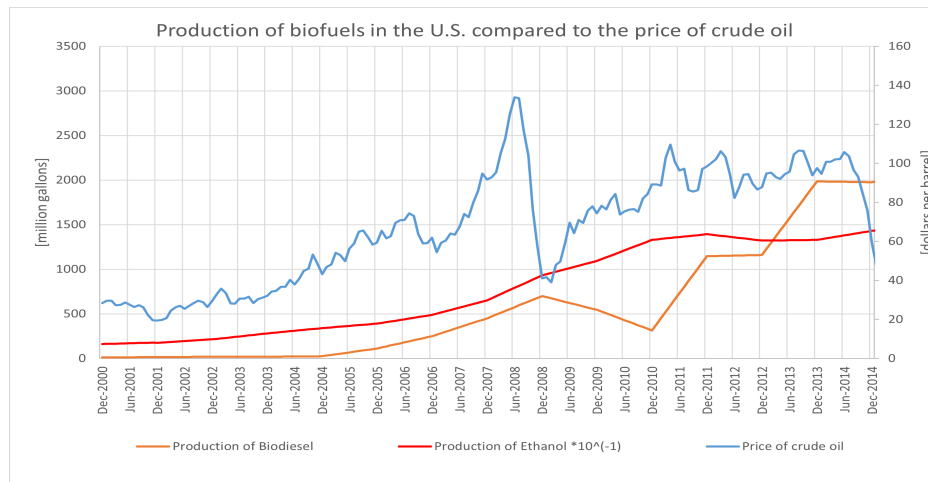


Figure 5: Increase in the production of biofuels in the U.S. vs price of crude

Biodiesel and ethanol are the most common fuel alternatives however, it is not possible to produce such biofuels in quantities able to fulfill the global demand without the generation of other problems. For example, the amount of corn, sugarcane or other plants needed for the production of alternative fuels would compete against the crops for food for land. To overcome the problem of land use, new methodologies have been investigated: algae-based biofuels would be able to increase productivity, unfortunately further research and optimization is still required in that field.

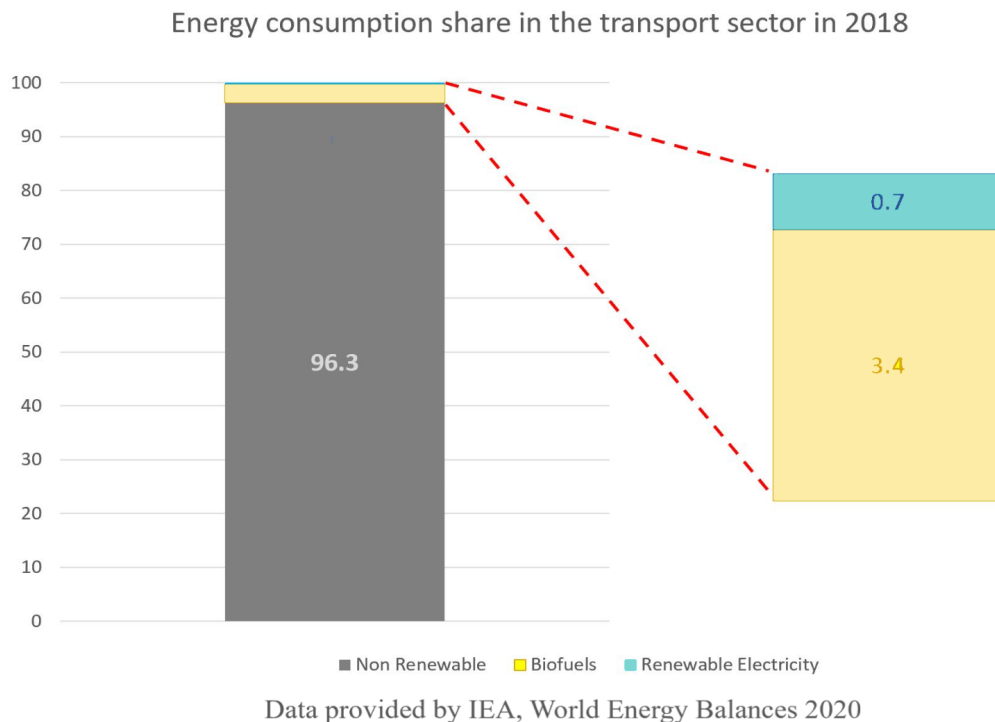


Figure 6: Energy consumption and renewable share in transport sector in 2018

Along with this issue, another problem in the energy sector is caused by the high share of energy produced from renewable energy sources such as solar or wind-based technologies. Even though those systems are necessary to reduce GHGs emissions, they are not reliable because they are highly dependent on atmospheric conditions. However, every year the power installed increases, reaching in 2018, in the European Union, the goal of providing just under one third (32%) of the electricity consumed from renewable sources [6]. Therefore, due to the low reliability of this technologies, the problem of balancing the electric grid gets worse every

year.

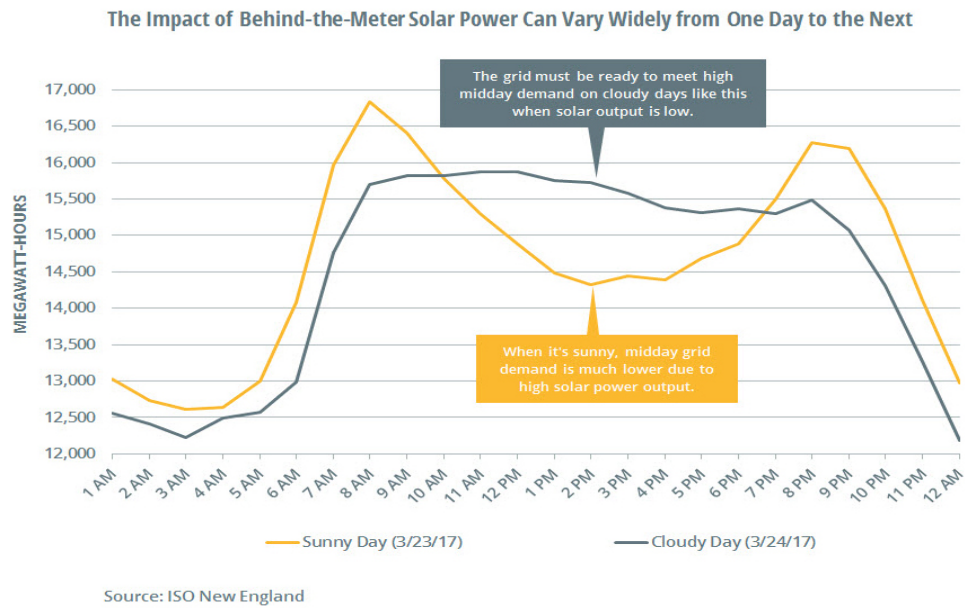


Figure 7: Electricity withdraw from the grid: sunny vs cloudy day comparison

For example, solar photovoltaic panels produce electricity during the hour when the sun is high in the sky, while they turn off during the hours of dark, or when the sky is cloudy.

This problem is particularly relevant during winter; indeed, the panels are over-sized and it could happen that in the hours of sun they produce electricity in excess and waste a part of that electricity while, when the intensity of the sun lights is not sufficient for the panels to produce energy, the system withdraws energy from the grid.

The surplus electricity can be stored in batteries or used in electrolytic cells to produce hydrogen, which, unfortunately is not easy to store at ambient conditions. Even though renewable energy systems are a good way to reduce GHGs emissions, the reduction of CO<sub>2</sub> can only be achieved by capturing the gas by means of carbon capture technologies. Some of these technologies are mature and they have been practiced since last few decades. The most common applications are based on amine solution that absorbs the gas from the stream rich in CO<sub>2</sub> flowing in the opposite direction, such systems were first patented in 1930s. In the years, many attempts have been made in order to optimize the already in-operation systems and new methodologies have been proposed, such as adsorption on activated carbon, absorption with blends of ionic liquids and separation with polymeric membranes [7].

After its capture, the CO<sub>2</sub> needs to be stored or used. The captured gas can be stored underground in depleted oil and gas fields, deep aquifers and unminable coal seams. Mineral carbonation is a permanent storage of carbon dioxide where it gets converted into stable carbonates. Some Carbon Capture and Storage (CCS) technologies are already working at commercial level [8], with the first CSS-equipped power station starting its operation in Saskatchewan, Canada. Unfortunately, the storage of CO<sub>2</sub> is not risk-free, in fact, gradual leakages could release it again into the atmosphere, as well as generate seismic events. Although underground storage is the fastest and large-scale solution in a linear economy, there is the need to create a circular carbon economy. This could be achieved by converting CO<sub>2</sub> into useful chemicals and energy products.

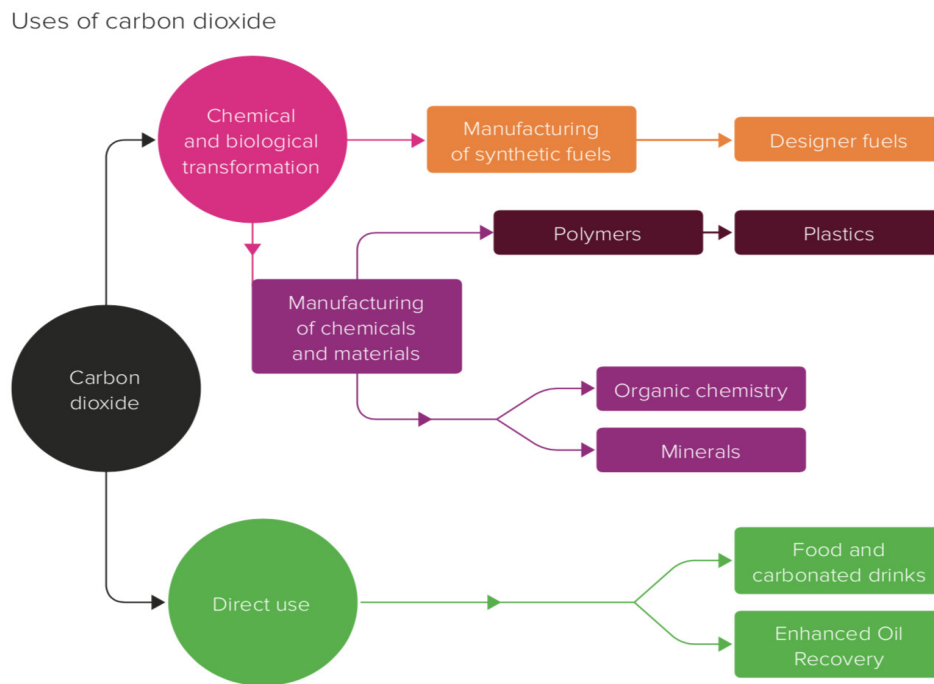


Figure 8: Possible uses of captured carbon dioxide [9]

Furthermore, despite the many advantages of CCS, it alone cannot meet the target of reducing CO<sub>2</sub> by 20 % by 2050. Indeed, all different strategies of energy management, circular economy, waste recycle and carbon capture storage and utilization should be followed at the same time.

Nowadays, the most common way to use CO<sub>2</sub> is through CO<sub>2</sub> Enhanced Oil Recovery (EOR) which could provide additional 500 thousand barrels of crude oil every day. This additional oil can be advertised as carbon-negative but, unfortunately, the majority of carbon dioxide

injected comes from natural sources [10]. Another way to utilize this gas is through its chemical conversion into fuels. Such conversion can be thermochemical or electrochemical, which uses excess electricity produced from renewable energy sources. The composition and characteristics of the output product would depend both on the technologies used and the working conditions at which the reactions take place.

To break the link between energy production and CO<sub>2</sub> emissions, for many years, attention has been focused on hydrogen and a “Hydrogen Economy” was theorized. Indeed, hydrogen is the most abundant element in the universe and it can be used as clean burning fuel, because during its reaction with oxygen it produces only water and it release a big amount of energy, or it could be used in fuel cells to generate electricity. The main issue of the Hydrogen economy is the huge monetary investment that would be required to modify the existing infrastructures or to create new ones. Furthermore, its storage handling is problematic because of its high volatility. An alternative to hydrogen is methanol, as discussed by Olah et al. in their book titled “Beyond Oil and Gas: The Methanol Economy” [11]. Indeed, even if biofuels and hydrogen would be optimized to completely cover all fuel and energy demand, there will still be the need for plastic and polymers that are used in many applications in chemical and pharmaceutical industries. This need could be fulfilled by methanol and dimethyl ether, from which it is possible to produce such chemicals.

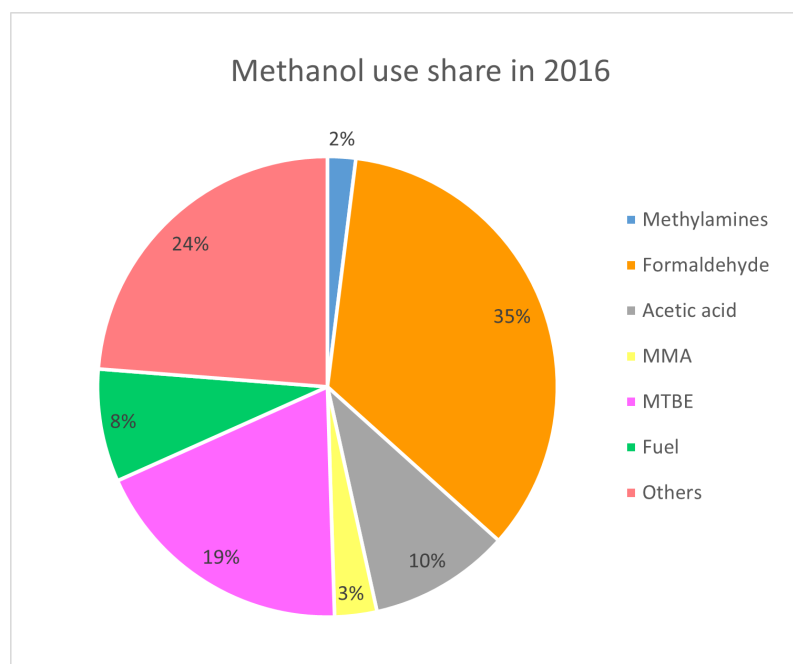


Figure 9: Global methanol application and transformation in 2016

Methanol has been considered, by Olah et al., the optimal product to meet the environmental target to a sustainable future. In fact, methanol is the only product able to replace petroleum in all its applications. Moreover, it is liquid at ambient conditions, therefore it is easily stored and it can be used in many applications in transport sector and chemical industry. It can also be used in many pre-existing systems and car engines [12]. Currently, methanol is mainly produced from syngas [13], which is generated from the incomplete combustion and reforming of fossil fuels. Another possible way to produce methanol is through carbon dioxide hydrogenation. This methodology has many advantages, such as the exploita-

tion of fossil fuels to more sustainable levels, and the lower the amount of CO<sub>2</sub> released into the atmosphere.

The main obstacle in the transition towards this new economy, based on CO<sub>2</sub> hydrogenation, is the high cost. Along with that, another key aspect is and the high amount of energy necessary to produce the required share of hydrogen and to capture the carbon dioxide. Indeed, the energy needed for producing the hydrogen necessary in the process accounts for the 80 % of the total energy needed, therefore it is fundamental that this energy comes from renewable sources. On the other hand, the energy required for the carbon capture depends on the source of the gas, for example, the atmospheric one is the most expensive to obtain. Usually, the majority of the energy needed for this section of the process is of the thermal kind and it is needed for the stripping of the molecule, once absorbed by the solution.

In order for an energy source to be considered a sustainable fuel alternative, it should have an energy return on investment (EROI) equal or higher than 3. The EROI is defined as the ratio between the energy possibly released by a fuel and the energy spent in the capture and delivery of this energy. For this reason, according to the up-to-date data presented in literature [14], the energy used to produce methanol from CO<sub>2</sub> needs to be reduced by a factor of 6 or more, compared to the current methodology. Significant efforts are required to reduce the energy needed through thermal integration and design optimization.

As already stated, the most common way to produce methanol is from syngas, through the Fisher Tropsch synthesis. The FT process, shown in Fig. 9, was first patented in the 1920s, and it has been used to produce hydrocarbon fuels and chemical products [15] for almost a century.

This well-known methodology, can be used as a reference to analyze the  $\text{CO}_2$  hydrogenation. In fact, the main difference between the two processes, is that FT synthesis converts syngas, which is mostly a mixture of carbon monoxide and hydrogen, with a relatively small amount of  $\text{CO}_2$ . However, this does not meet the sustainability objective, since syngas is usually derived from coal, from which the process takes the name of carbon-to-liquid (CTL), or natural gas-to-liquid (GTL).

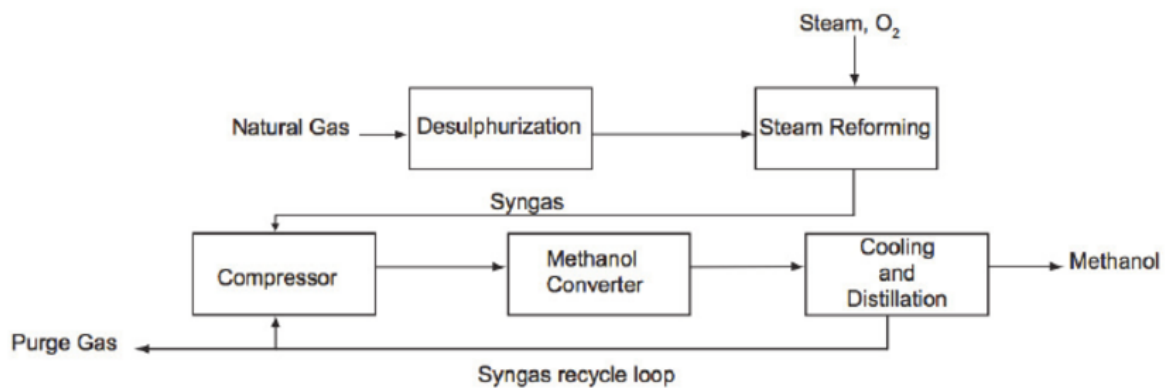


Figure 10: Simplified scheme for methanol synthesis from syngas [15]

Beside this difference, the main reactions, such as gas-water shift, carbon monoxide and carbon dioxide hydrogenation, are similar in the two processes. Due to high stability of the molecules involved, the reactions take place on a catalyst.

Water-gas shift:



Carbon dioxide hydrogenation:



Carbon monoxide hydrogenation:



All three reactions are present in the process for producing methanol both from syngas and from  $\text{CO}_2$ . However, due to the slow kinetic and small amount of CO present in the mixture, in the case where the starting component is carbon dioxide, reaction (1.3) is often excluded from the kinetic models [18]. Many catalysts have been proposed for this application. One of the commonly used catalyst, is  $\text{CuO}/\text{ZnO}/\text{Al}_2\text{O}_3$ , which favors the hydrogenation of carbon dioxide over the one of carbon monoxide [17]. In fact, CO generates  $\text{CO}_2$  through the water-gas shift, which is later transformed into methanol.

In mixtures composed of only  $\text{CO}_2$  and  $\text{H}_2$ , the reverse water-gas shift reaction competes with the hydrogenation reaction, leading to the presence of undesired CO in the output stream. In order to avoid this and optimize methanol production, the reaction conditions must be kept at optimal values. This is particularly difficult in the case of temperature since the reactions involved are strongly exothermic. Indeed, one of the biggest technical challenge is to remove the large amount of heat generated in the reactor [19]. Later, a thermal integration is performed with that power: for example, it could be used for the stripping in the carbon capture process.

The thermal integration could achieve a significant reduction in energy waste and, therefore, improve the EROI index.

With the help of a mathematical model, it is possible to describe the processes inside the reactor, assess the optimal reaction conditions, and describe the influence of input parameters on the results. Commercial software is able to provide data about the dynamic, thermal and chemical behavior of the components inside the selected domain. One of these software is COMSOL; it is able to simulate multi-physics phenomenon, and to provide results for both stationary and time problems.

## CHAPTER 2

### PRODUCTION OF METHANOL

Methanol is mostly produced from syngas generated from fossil fuel reforming. This makes the process not sustainable since its production depends on the depletion of non-renewable resources. To overcome this issue, methanol could be produced with the hydrogenation of carbon dioxide through thermo- and electro- catalytic processes.

Methanol can be used as a fuel in traditional engines or as a starting compound for the chemical industry. Furthermore, it can be transformed into dimethyl ether (DME) through dehydrogenation, which, in turn, can be used to produce a wide range of products. The methanol production from  $\text{CO}_2$  is a strongly exothermic process. Unfortunately, when the temperature exceeds a specific threshold, the selectivity of the catalyst towards methanol is compromised and the stability of the materials composing the reactor is endangered. Therefore, the management of temperature in the process is of particular interest. Along with the carbon dioxide hydrogenation reaction itself, the overall process is divided into carbon capture, production of hydrogen and separation of the methanol produced.

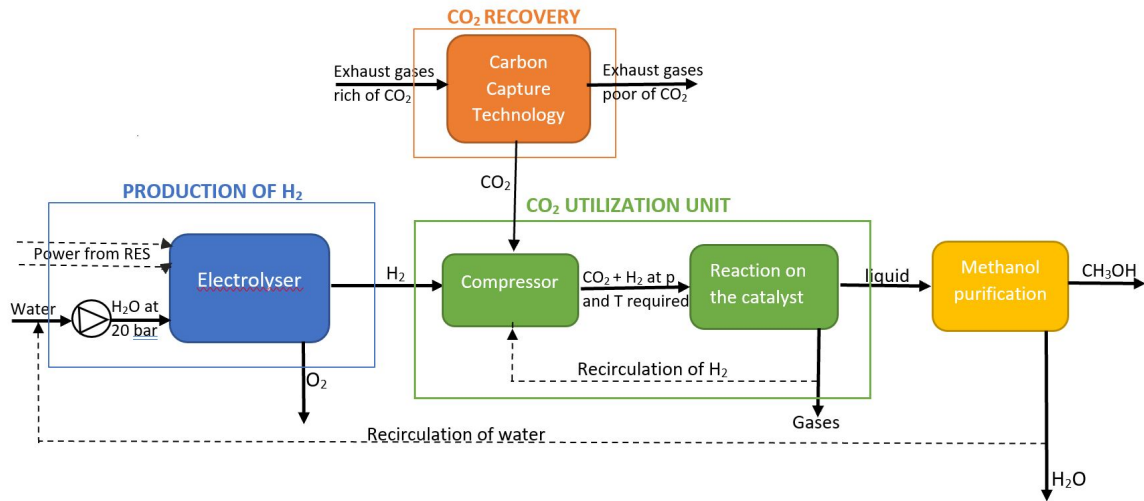


Figure 11: Schematic process for production of  $\text{CH}_3\text{OH}$  from  $\text{CO}_2$  rich stream

### 2.0.1 Possible Sources of $\text{CO}_2$

Carbon dioxide can be captured from natural and anthropogenic sources. Furthermore, in recent years, new technologies have been proposed to extract  $\text{CO}_2$  from the atmosphere via Direct Acquisition Capture (DAC) technology. This last system could achieve negative emission of GHGs; however, because of its high cost, it cannot be considered as a possible alternative to obtain large quantities of carbon.

Ocean water could also be used as a  $\text{CO}_2$  source. When the gas is extracted from that, the methanol produced takes the name of "Sea fuel". The most efficient carbon capture technology depends on the source of the stream that needs to be treated. Also, different technologies

work better at different temperatures, pressures and mixture compositions. Therefore, the cost of the captured CO<sub>2</sub> varies in accordance to the stream conditions and technology used. For example, the cost of capturing CO<sub>2</sub> from carbon rich flue gases, is several order of magnitude less expensive than that of capturing it from the atmosphere. This is due to the different CO<sub>2</sub> concentrations in the two sources: in gases from fossil fuels combustion, the volumetric concentration is usually around 10 to 15%, while, in the atmosphere, it is slightly higher than 410 ppm. Indeed, for sources with low CO<sub>2</sub> concentrations, the cost is higher because the energy needed to extract the gas is higher and the technologies are more sophisticated.

According to one recent estimate, the cost of extracting CO<sub>2</sub> from the atmosphere is around \$600 per ton of CO<sub>2</sub>. However, some scientists hypothesize that chemical plants in the future could reduce that cost below \$100 per ton, which could make synthetic fuels from the atmosphere a reality [20]. At that price, the carbon captured from the atmosphere, could be used in many applications and return good profit to investments. DAC has no geological constraints, therefore it could be done anywhere, and it would create an anthropogenic close life cycle for CO<sub>2</sub>. Even though this approach will be preferable in the future, right now, other technologies are chosen because of their lower cost. For example, the cost of CO<sub>2</sub> captured from post-combustion power plants using monoethanolamine (MEA), the benchmark for chemical absorption, is currently over US\$60 per metric ton of CO<sub>2</sub> [21]. This cost is 10 times lower than that of capturing CO<sub>2</sub> from the atmosphere.

In the production of methanol from carbon dioxide, the cost and energy investment are the key aspects; therefore, for this specific application, a stream rich in CO<sub>2</sub> must be used, such as

flue gases from a cement factory or from a power plant.

## 2.1 Carbon Capture Technologies

The technologies used to capture the CO<sub>2</sub> present in a mixture of gases are many. They differ for the range in which they operate, the materials they are made of, and the cost and efficiency. Despite their great efficiencies, some CC technologies do not match the conditions at which the most common streams of flue industrial gases exit the plants. In fact, with the technologies now in use, it is possible to capture up to 95 % of the CO<sub>2</sub> present in a stream, however this percentage depends on the characteristic of the stream. Unfortunately, the net carbon capture must consider that, for the capture itself, some energy is needed. Therefore, considering also this aspect, the net capture of CO<sub>2</sub> ranges between 80 and 90 % [22].

A commercial CC technology is based on the adsorption of the gas on a solid substrate. The regeneration of the adsorber can be done by increasing the temperature or decreasing the pressure of the system, this method is used for high concentrations of CO<sub>2</sub>. This technology has high loading capacity at ambient conditions and low energy needs. Examples of physical adsorbent are activated carbon, zeolite, silica membrane and MOFs. CO<sub>2</sub> can also be captured via membrane technique. These systems use the Knudsen diffusion principle and the Fick's molecular diffusion to separate CO<sub>2</sub>. However, it can only be used for streams with very high CO<sub>2</sub> concentration, for example to separate the CO<sub>2</sub> from a natural gas stream.

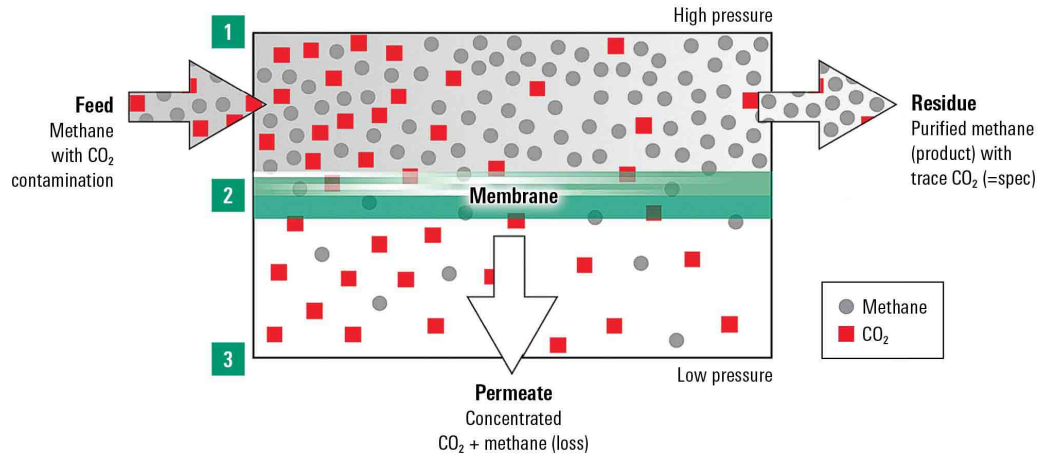


Figure 12: Working principle of a membrane CC technology [23]

Between all the technologies, carbon absorption is the most mature one. Absorption could be chemical or physical. The latter follows Henry's law and the interactions between gas and absorber are of the Van der Waals type. This kind of capture is favored at high pressures and low temperatures.

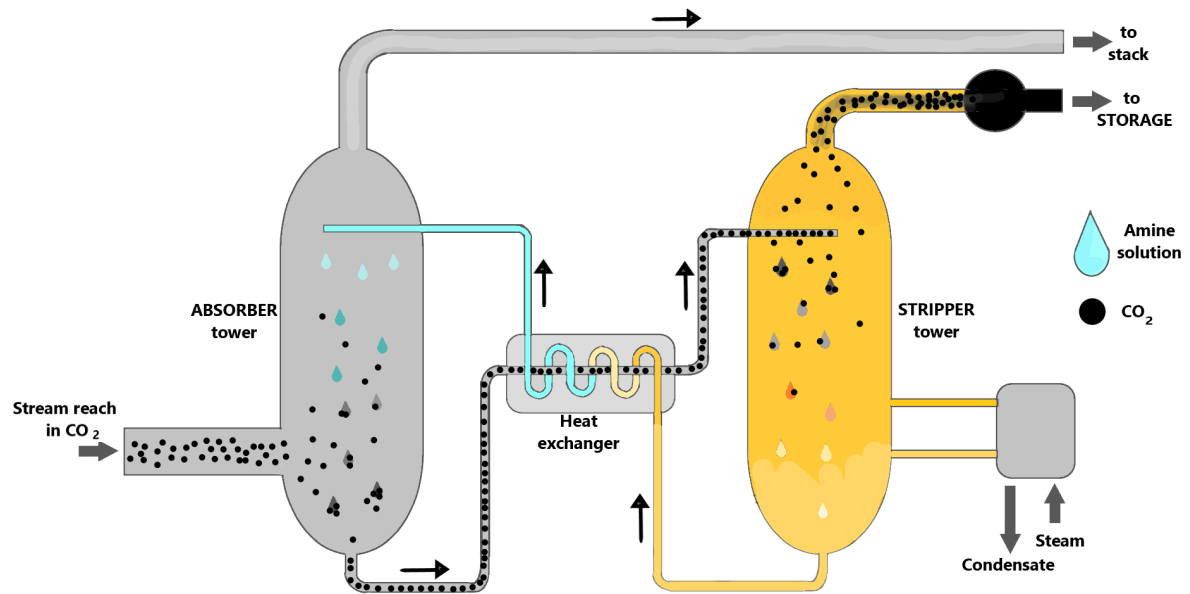


Figure 13: Scheme of the process of CO<sub>2</sub> capture by absorption

The chemical absorption of CO<sub>2</sub> with a diluted solution of monoethanolamine, described in Fig. 13, is perhaps the most mature and reliable technology [24]. The MEA-based absorption can be used in the methanol production process because it can absorb CO<sub>2</sub> at pressure and temperature close to ambient condition and at moderate concentrations. Furthermore, this system has high reliability and low costs. In carbon capture by amine absorption, the stream needs to be at the temperature of 40 - 60 °C and introduced into the absorber where it bonds with the solvent.

After the absorption, the solution must be recovered and the CO<sub>2</sub> separated from the absorbent. This step of the process, known as stripping, is the most energy intensive one.

To reduce the amount of thermal energy needed, new methods have been studied, such as blends of MEA and ionic liquids. When using this technique, an additional step should be performed before the absorption: NO<sub>x</sub> and SO<sub>x</sub> must be eliminated from the flue gases, since they could compromise both the carbon capture and the catalyst used in the methanol reactor. Those are also related to thermal degradation risk in the stripping process. In fact, it could lead to the production of potentially toxic compounds, due to nitrosation and nitration, two reactions that are favored at high temperature.

After its capture, CO<sub>2</sub> must be transported at supercritical conditions, therefore it is introduced into the pipelines at a temperature of 31°C or above and a pressure of 7.4 MPa. Usually, it is pressurized at 80 bars and pumped into pipelines, while, for longer distances, it is more convenient to use ship tanks, where it is transported in liquid state at 20 bars and -2°C. The cost of transport is in the range between 5 and 15 \$/tCO<sub>2</sub> /km, varying according to the distance and the method used. For this reason, it is necessary to produce the required CO<sub>2</sub> as close as possible to where the methanol is produced. If the inlet stream rich in CO<sub>2</sub> is intermittent, in order to avoid stopping the plant, a tank must be present to store a quantity of CO<sub>2</sub> that can be used as buffer, to never stop the reactor. In fact, the process takes time to reach its operation conditions and starting and stopping the process frequently could lead to damage of the components of the system.

### 2.1.1 Comparison between Pure MEA and Ionic Liquids Blend

As already stated, the most mature technology for carbon capture is the absorption with pure MEA. It represents the most economic and a reliable option; but requires high amount of thermal energy to regenerate the sorbent. To reduce the energy for stripping, new methodologies are being investigated [24]. A promising alternative to pure MEA sorbent, is the ionic liquid blend solution. This new sorbent requires less thermal energy for stripping, even the energy must be provided at higher temperature.

The performance of a ionic liquid blend [Bpy][BF<sub>4</sub>] has been studied by Santarelli and Fino et al.[24], using the double column scheme with recycle of solvent. Both in the case of ionic blend and of pure MEA solvent, the stream exiting the absorber column, poor in CO<sub>2</sub> could be recirculated but this would lower the efficiency of the process, because the concentration of the inlet stream would be lower. Using the same initial stream, it is possible to compare the performances of the two solvents, taking the pure MEA as a reference. Indeed, starting with the benchmark case, it is possible to evaluate how the power needed for the stripping of the solvent is effected by the use of the two different solvents.

TABLE I: COMPARISON BETWEEN PURE MEA AND BLEND [Bpy][BF<sub>4</sub>]

	<b>7m MEA</b>	<b>Blending with [Bpy][BF<sub>4</sub>]</b>
Heat of regeneration	1.33 kWh/kgCO <sub>2</sub>	0.97 kWh/kgCO <sub>2</sub>
Temperature	120 °C	140 °C
Reduction in energy for regeneration	0%	- 27%

As shown in Table I, ionic blend would require 27 % less energy for stripping, compared to the MEA case.

Unfortunately, the ionic blend is still not a mature technology and the cost and risk on the investment would be higher. This would result in a higher overall cost of the methanol produced. However, this solution has the potential to be launched on a commercial level, which will further reduce the cost. Furthermore, thanks to the thermal integration with the power extracted from the reactor, could drastically reduce the EROI of the produced methanol.

## 2.2 Electrolyzer

From decades, it has been possible to produce hydrogen from the electrolysis of water. To make this process sustainable, the electricity needed to split the water molecules into H<sub>2</sub> and

O<sub>2</sub>, should be provided by renewable energy sources such as wind turbine, photovoltaic panels and geothermal plants. In 2020, less than 4% of hydrogen was produced via electrolysis, while the majority was generated through steam reforming of natural gas. This is mostly due to the higher costs of the renewable electricity itself and its unreliability.

There are three main methods to produce hydrogen from water, depending on the materials used and the operation mode [25]. Two of them, namely the polymer membrane electrolyzer (PEM) and the alkaline electrolyzer, are already implemented at commercial scale. The alkaline electrolyzer is composed of two electrodes separated by an electrolyte, which transports OH<sup>-</sup> ions from cathode to anode. The alkaline solution is often made of diluted sodium or potassium hydroxide at temperatures in the range of 50 to 100 °C.

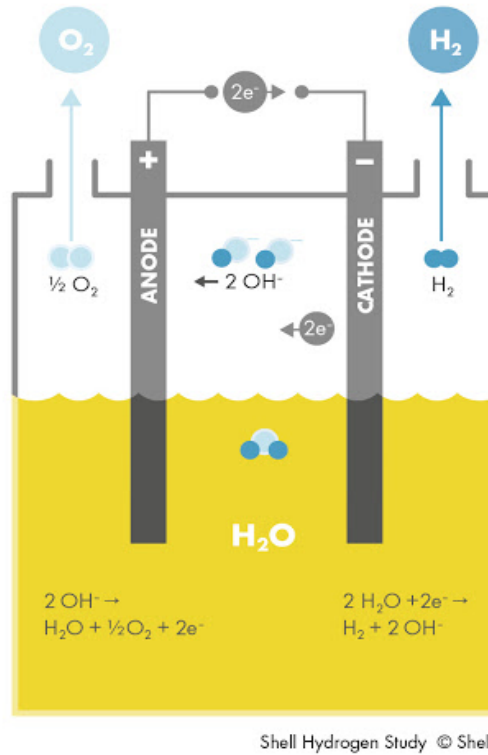


Figure 14: Schematic of an Alkaline Electrolyzer [26]

PEM electrolyzer works in the same temperature range, while the electrolyte is made of solid specialty plastic, where  $\text{H}^+$  ions cross the membrane and reach the cathode, where they recombine with the electrons.

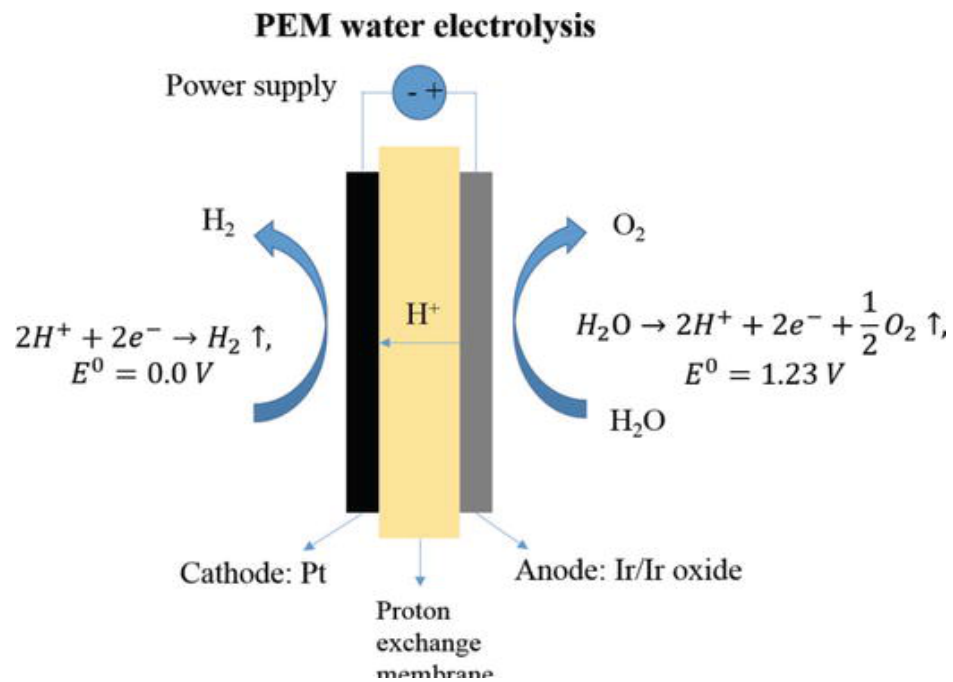


Figure 15: PEM electrolyzer principle [27]

The solid dioxide electrolyzer (SOEC) is still in the development phase. In this technology,  $O^{2-}$  ions are transported to the anode through a solid ceramic material. This system works at temperature of 700 to 800 °C, but requires lower electricity consumption.

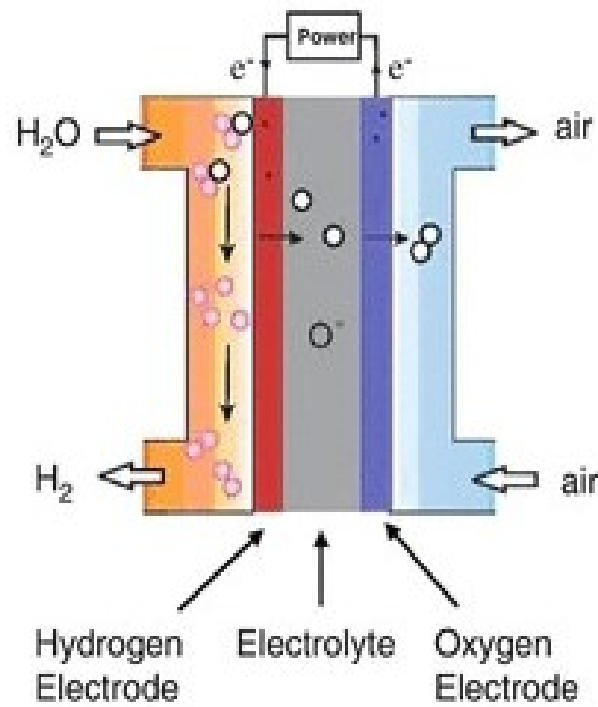


Figure 16: Solid Oxide electrolyzer principle [28]

In conclusion, alkaline electrolyzer is the most mature technology. Compared to PEM, it is less efficient; however, in order to reduce the overall cost, alkaline electrolyzers are preferred for the present application, since hydrogen generation is the most expensive part of the process for producing methanol. Moreover, in order to compete with the steam reforming process, the research should focus on reducing the capital costs of the electrolyzer itself and on improving the energy efficiency, as well as to develop more flexible systems, which can adapt to intermittent

and fluctuating power supply, typical of many renewable energy systems.

### **2.2.1 Source of Electricity**

The production of methanol from CO<sub>2</sub> is a process that aims at reducing the concentration of GHGs in the atmosphere. For this reason, the source of electricity necessary to produce H<sub>2</sub> should be selected with special care. The electricity should be, at the same time, cheap and sustainable. Therefore, it is necessary to select an optimum option from the many mature renewable energy technologies. A key aspect is the continuity at which the electricity is supplied, in fact, it is better to run the process in steady conditions and avoid many starts and stops. For this reason back up storage of CO<sub>2</sub> and H<sub>2</sub> are often present in the plant.

The cost of electricity from solar and wind applications have continued to fall in the last decade, complementing the more mature bioenergy, geothermal and hydropower technologies. The cost of electricity from solar photovoltaic panels fell 13% each year, reaching the value of USD 0.068 per kWh, in 2019. At the same time, the cost of wind energy had a decrease of 9% per year [29].

TABLE II: TECHNOLOGIES TO PRODUCE RENEWABLE ELECTRICITY

<b>Technology</b>	<b>Cost of electricity</b>	<b>Intermittent operation</b>
Geothermal Plant	USD 0.08/kWh	NO
Hydropower Plant	USD 0.055/kWh	Generally, NO
Solar Photovoltaic	USD 0.068/kWh	YES
Wind Turbine	USD 0.053/kWh	YES
Concentrating Solar Plant	USD 0.182/kWh	YES

However, if possible, options such as geothermal and hydropower should be preferred because they work in continuous manner without unpredictable start-and-stop.

### **2.2.2 Intermittent Electrolyzer Working Conditions**

For optimum operation, electrolyzers should work continuously. In fact, they can only work in a specific operation window. In those systems, the power should be maintained above 10 or 25 % of the nominal value, otherwise the low current density would produce high quantities of impurity in the output stream. These impurities could overcome the safety range admissible of 2%. For this reason, when the power provided to the system is too low, it immediately shuts

down, because in the range of impurity from 4 to 96 %, both  $H_2$  and  $O_2$  are within explosive limits.

When using intermittent renewable energy [30], the system could be shut down multiple times per day. The frequent start-and-stops, produce a faster degradation of the alkaline electrolyzer. The deterioration of electrodes and the transient operation, reduce the quality and quantity of the output gas and the expected lifetime of the component. When the production of hydrogen is interrupted and the buffer tanks are empty, the whole process to produce methanol should be stopped.

When using a technology such as photovoltaic systems or wind turbine, a battery could be added to the system to store the excess electricity, produced during the hours when the production exceeds the demand. This energy could be used later to reduce the risk of stopping the production, during the hours of dark of low intensity wind.

### **2.3 Reactor**

Carbon dioxide hydrogenation can occur either under adiabatic or isothermal conditions. At present, methanol is mostly produced in adiabatic reactors (60 %), while the 27 % of it, with Lurgi or quasi-isothermal reactions [36]. It is possible to use the adiabatic reactors in a quench reactor scheme or divide the process with a series of inter-stage refrigeration. On the other hand, the temperature in a quasi-isothermal reactor is controlled via a cooling system. The isothermal process is characterized by a higher methanol yield than that of adiabatic reactors,

because the temperature in the reaction zone is usually lower. However, the adiabatic model has a simpler reactor scheme [32].

In the quasi-isothermal reactor, the heat produced must be removed, requiring the flow of a refrigerant fluid. To keep the temperature of the reaction constant, the refrigerant fluid, generally water, is boiling, so that it absorbs thermal energy, but its temperature does not change. The two types of reactors used are the packed bed or shell-and-tubes type (Fig. 17).

The latter can remove a higher amount of thermal energy, due to its larger heat exchange surface.

The mixture of  $\text{CO}_2$  and  $\text{H}_2$  flows inside the inner tubes, where the catalyst is present. The size of the catalyst pellets will modify the heat transfer coefficient and the kinetic of the process. It is, therefore, extremely important to select the optimal dimensions and other characteristics of the pellets.

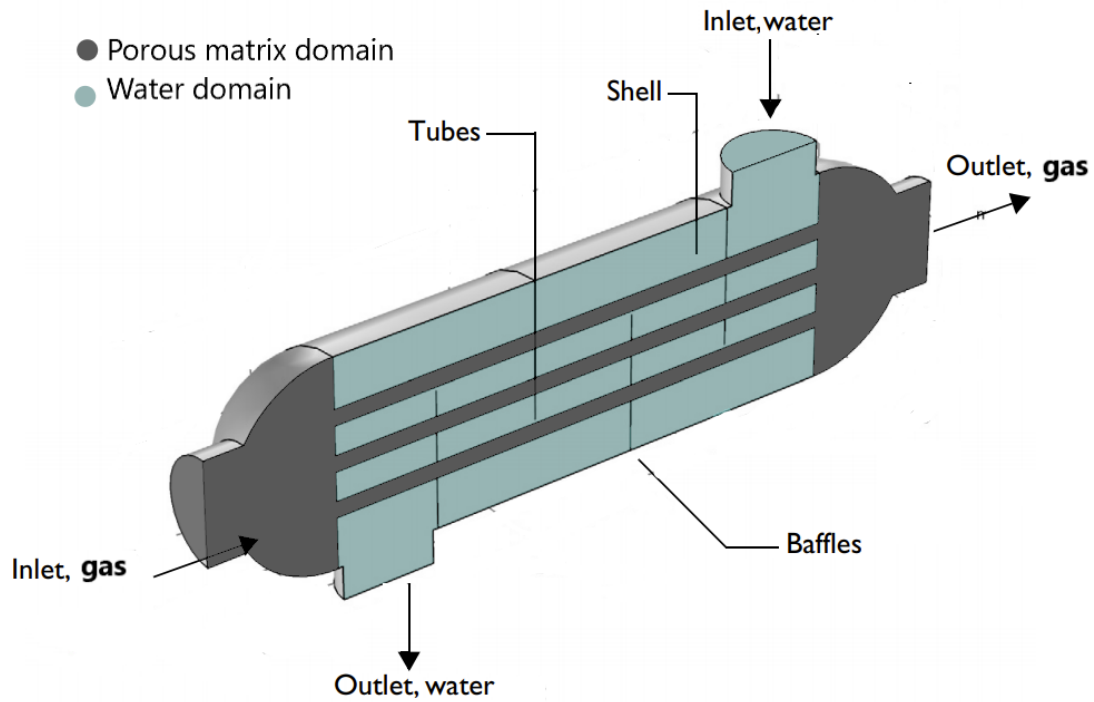


Figure 17: Schematic of a shell-and-tubes reactor

#### 2.4 Methanol separation

The outflow from the reactor, must be treated to separate methanol from the rest of the components in the product stream, which is still rich in carbon dioxide and hydrogen. Therefore, those gases must be separated and recirculated. This can be done by using a series of separation columns, as indicated in Fig. 18. Indeed, the first column works at the pressure of 10 bar and 45 °C so that water and methanol are liquid and easily separated from the gases. After that, methanol is separated from the water at 2 bar pressure. This process is quite simple because

methanol has a density of 0.79 times that of water. Then, the methanol should be stored in closed tanks in a safe environment. Indeed, the upper flammability limit of methanol is 36 percent by volume (vol%) and it burns with a transparent flame, therefore, it is essential that fire detection, alarm, response, and suppression systems are rapid and effective.

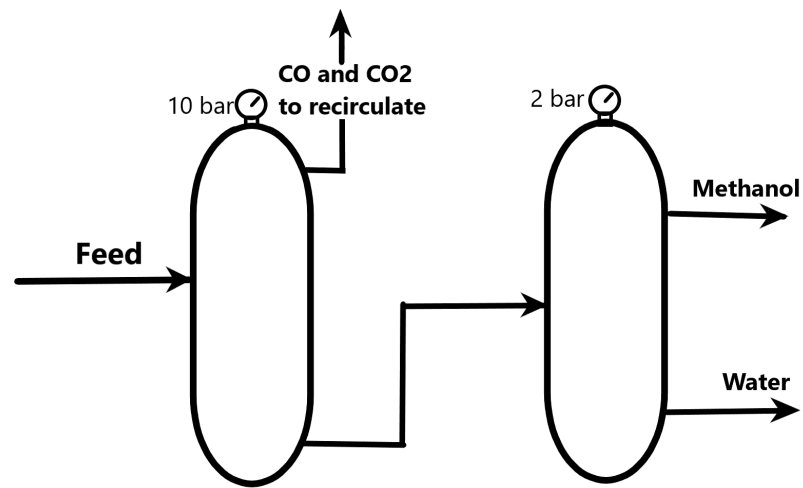


Figure 18: Schematic of the separation columns

## CHAPTER 3

### CATALYST CHARACTERIZATION AND KINETIC MODEL

Methanol is mostly produced from syngas obtain from fossil fuels. This process has been used for decades, and its kinetic has been studied and described by many scientists [18]. The reaction takes place in the presence of a catalyst.  $\text{CuO}/\text{ZnO}/\text{Al}_2\text{O}_3$  is a commercial catalyst often used in this process, and it provides optimal performance at temperatures between 200 and 300°C, and pressures between 5 to 10 MPa. Generally, this catalyst is composed of 60% CuO by weight, 30% ZnO and 10%  $\text{Al}_2\text{O}_3$ .

In fact, this catalyst favors the generation of methanol from  $\text{CO}_2$  rather than from CO, due to the Water-Gas Shift reaction [34], Eq. (1.1). Methanol is then produced, on a catalyst, from the  $\text{CO}_2$  hydrogenation, Eq. (1.2), and the overall reaction for methanol synthesis can be described as a linear combination of the previous two, Eq. (1.3). This approach is known as the "indirect conversion" of syngas into methanol. In contrast, the direct approach consists of starting directly from  $\text{CO}_2$  and  $\text{H}_2$  to produce  $\text{CH}_3\text{OH}$ . With further research, this approach is expected to be technically competitive with the one that starts from syngas. While, for the process of conversion of syngas into  $\text{CH}_3\text{OH}$ , many data are available and they can describe accurately the kinetics model, the carbon dioxide hydrogenation kinetics is still an active field of research.

The chemical recycling of  $\text{CO}_2$  into methanol, would provide a sustainable source for transport fuels, for storing energy, and a feedstock for producing ethylene and propylene. However,

CO<sub>2</sub> hydrogenation, produces water as a by product, in higher quantity than that that would have been produced using syngas. Another disadvantage is that the condition for producing methanol from CO<sub>2</sub> are less favorable than the ones for producing it from syngas. For example, at 200 °C with a commercial catalyst, CO<sub>2</sub> hydrogenation yields 40 % of methanol, while with syngas, the yield is more than 80 %. This is due to the fact that CO<sub>2</sub> is a very stable molecule; therefore, it is necessary to overcome its thermodynamical barrier by means of an active catalyst, which must be used in a range of temperature above 250 °C in order to obtain good activity.

Different catalysts have been analyzed for the CO<sub>2</sub> hydrogenation and many kinetic models have been proposed [34]. A preferred catalyst one is CuO/ZnO/Al<sub>2</sub>O<sub>3</sub>, which is the same used to produce methanol from syngas. This catalyst has good selectivity towards methanol, therefore, the amount of CO present at the output due to the Reverse Water-Gas Shift (RWGS) reaction is small. Furthermore, it has good stability, long expected lifetime and fast kinetic even at relatively low temperatures. However, the size of the catalyst impacts both the mass transfer of gas and the temperature increase. For this reason, the size and number of pellets must be selected with care. Also, while the high temperature helps the activation of CO<sub>2</sub>, an excessively higher temperature could produce unwanted CO, which is generated by the reverse water-gas shift reaction. This reduces the methanol output and increases the output of water, which can cause the crystallization of Cu and ZnO, and thus lead to the deactivation of catalyst. The properties of the catalyst measured under the reaction conditions of 523 K and 5.0 MPa [34] are reported in Table III.

TABLE III: CHARACTERISTIC OF CuO/ZnO/Al<sub>2</sub>O<sub>3</sub> CATALYST

Catalyst	Surface area	Average pore	CO <sub>2</sub> conversion	selectivity [mol %]
	[m <sup>2</sup> /g]	size [nm]	[mol %]	MeOh
CuO/ZnO/Al <sub>2</sub> O <sub>3</sub>	106.9	31	26.8	93.5

The methanol selectivity data shown in Table III, are lower than 95 %, therefore, products other than methanol are produced.

### 3.1 Kinetic Model

The kinetic model depends on the catalyst used and the conditions at which the reaction takes place. For the catalyst, as discussed earlier, and the optimal conditions of 250 °C and 5 MPa, Vanden Bussche and Froment [18] have developed a kinetic model that considers only two independent reactions: the carbon dioxide hydrogenation and the reverse water gas shift. In fact, the carbon monoxide hydrogenation is a linear combination of the previous two, while other side reactions can be neglected thanks to the high selectivity of the catalyst.

Following the Vanden Bussche and Froment approach, the reaction rates of the process are expressed by Eq. (3.1) and Eq. (3.2), which describe respectively the kinetic of reaction (1.2) and the reverse of (1.1).

$$r_{\text{CO}_2\text{hydrogenation}} = \frac{k_1(P_{\text{CO}_2}P_{\text{H}_2})\left[1 - \left(\frac{1}{K_{eq,1}}\right)\frac{p_{\text{CH}_3\text{OH}}p_{\text{H}_2\text{O}}}{p_{\text{CO}_2}p_{\text{H}_2}^3}\right]}{\left(1 + k_2(P_{\text{H}_2\text{O}}/p_{\text{H}_2}) + \sqrt{k_3p_{\text{H}_2} + k_4p_{\text{H}_2\text{O}}}\right)^3} \quad (3.1)$$

$$r_{\text{RWGSreaction}} = \frac{k_5P_{\text{CO}_2}\left[1 - (K_{eq,2})\frac{p_{\text{CO}_2}p_{\text{H}_2\text{O}}}{p_{\text{CO}_2}p_{\text{H}_2}}\right]}{1 + k_2(P_{\text{H}_2\text{O}}/p_{\text{H}_2}) + \sqrt{k_3p_{\text{H}_2} + k_4p_{\text{H}_2\text{O}}}} \quad (3.2)$$

The coefficients of the kinetic model for a process that takes place on a fixed bed reactor with the catalyst density of  $1200 \frac{\text{kg}}{\text{m}^3}$  and the bed porosity of 0.45 are reported in Table IV [37].

TABLE IV: KINETIC PARAMETERS OF THE REACTIONS

	A		B	
$k_1$	1.07	$mol/(kg_{cat} \cdot s \cdot bar^2)$	36,696	$J/mol$
$k_2$	$3.45 \times 10^3$	—	0	$J/mol$
$k_3$	0.499	$bar^{-0.5}$	17,197	$J/mol$
$k_4$	$6.62 \times 10^{-11}$	$bar^{-1}$	124,119	$J/mol$
$k_5$	$1.22 \times 10^{10}$	$mol/(kg_{cat} \cdot s \cdot bar)$	-94,765	$J/mol$
$k_6$	$5.35 \times 10^{13}$	$kmol/(kg_{cat} \cdot h)$	-143665.92	$J/mol$
$K_{CH_3OH}$	$5.39 \times 10^{-4}$	$m^3/kmol$	70,560.918	$J/mol$
$K_{H_2O}$	$8.47 \times 10^{-2}$	$m^3/kmol$	42,151.98	$J/mol$

The parameters are expressed in an Arrhenius equation, as reported below.

$$k = Ae^{-\frac{B}{RT}} \quad (3.3)$$

Also the constants of equilibrium,  $K_{eq,1}$  and  $K_{eq,2}$ , have an Arrhenius type dependency on temperature and are expressed by Eq. (3.3) and (3.4).

$$\log_{10}K_{eq,1} = \frac{3066}{T} - 10.592 \quad (3.4)$$

$$\log_{10} \frac{1}{K_{eq,2}} = \frac{-2073}{T} + 2.029 \quad (3.5)$$

## CHAPTER 4

### MATHEMATICAL MODEL

Complex physical processes are generally represented by suitable mathematical models, which often comprise of a system of differential equations. Since in many cases, these equations cannot be solved analytically, the solution is obtained with the help of numerical methods. This allows us to simulate the behavior of the process/system, and use numerical results in the design and optimization of real systems. Indeed, this can speed up the decision-making process, and provide a set of optimal parameters to use when starting a new plant. However, before using the results of such models, the models must be validated using appropriate data from experiments. Then, the numerical simulations can be used for further analysis, as well as for a parametric study.

Several commercial software are now available for such numerical studies. COMSOL is one of these software: it allows multi-physics simulations by solving coupled systems of partial differential equations. The software solves the mass and energy balance in order to find a stable operating point on specified parameters. Then, the parameters can be modified in order to determine the optimal conditions at which the physical phenomena should occur. While the use of models introduces approximations and assumptions, this approach could still describe the system behavior and properties for a range of temperature and pressure that cannot be otherwise achieved for real processes without the construction of extremely expensive plants.

#### 4.1 Geometry Simplification

The goal is to create a model able to describe how the carbon dioxide hydrogenation evolves in the selected reactor. It is extremely important to keep temperature and pressure, in the reactor in ranges where the catalyst performs at its optimum. Temperature can be maintained in such range by the use of a refrigerant fluid that flows in the outer shell of the reactor. Among all possible reactors able to exchange thermal energy with a cooling fluid, the shell and tubes configuration is one of the most efficient. For this reason, a shell and tube fixed bed reactor has been selected for this specific case.

The shell and tubes reactors are designed in order to obtain a similar evolution of the process in every tube. Therefore, to study the system, it is sufficient to analyze what happens just inside one of the tubes. Every possible interaction with the other tubes can be described by applying boundary conditions able to take into account what happens outside the analyzed domain. This simplification of the system leads to a simpler mathematical model, which can reduce the computational cost.

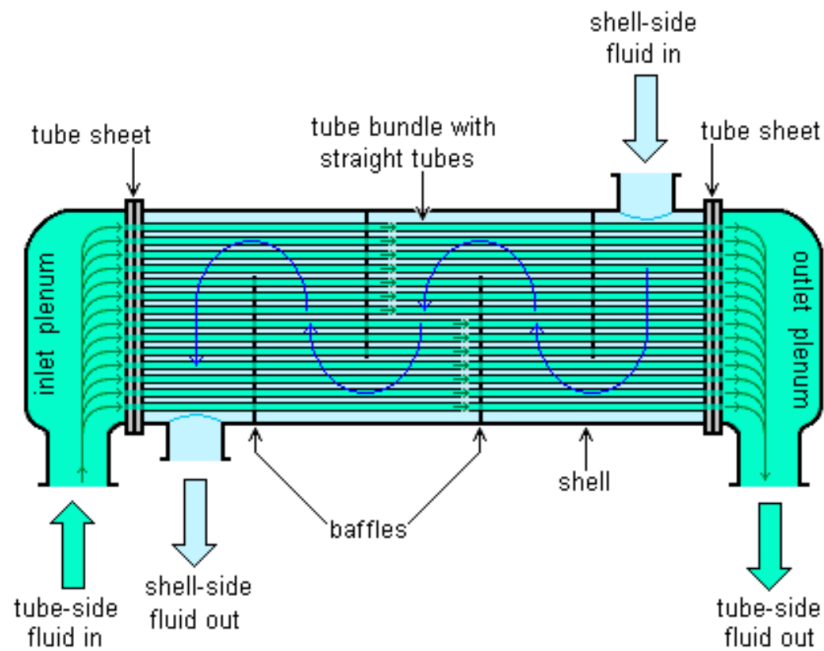


Figure 19: General scheme of a shell and tubes reactor [35]

#### 4.2 Model of the One-Dimensional Pseudo-Homogeneous Fixed-Bed Reactor

To describe how the process evolves along the axis of the reactor, the simplest model that can be implemented is the one-dimensional pseudo-homogeneous model [40]. In this model, the process takes place along the axis of the tube and no radial effects are considered. Energy and mass balance are the key equations that describe the process, while the reactions take place with the reaction rates described by Eq.(3.1) and Eq. (3.2).

The gaseous stream is considered as a mixture of ideal gases. Then we can use the equation of state, Eq. (4.1).

$$\frac{p}{\rho} = \frac{R_{const}}{M} \cdot T \quad (4.1)$$

For a mixture, the molar mass is the sum of the molar mass of each gas, multiplied by its molar fraction in the mixture.

$$M_{mix} = \sum_i x_i \cdot M_i \quad (4.2)$$

Then, the specific heat capacity and the thermal conductivity can be evaluated.

$$C_{p,mix} = \sum_i \omega_i \cdot \frac{C_{p,i}}{M_i} \quad (4.3)$$

$$k_{mix} = 0.5 \left( \sum_i x_i \cdot k_i + \frac{1}{\sum_i \frac{x_i}{k_i}} \right) \quad (4.4)$$

TABLE V: PARAMETERS OF EQ. (4.1) TO EQ. (4.4)

$\rho$	gas density	$\left[\frac{kg}{m^3}\right]$
$p$	pressure	$[Pa]$
$T$	absolute temperature	$[K]$
$R_{const}$	gas constant	$\left[\frac{J}{K \cdot mol}\right]$
$M$	molar mass	$\left[\frac{kg}{mol}\right]$
$n$	number of moles	$[mol]$
$x$	molar fraction	$\frac{n_i}{\sum_i n_i}$
$\omega$	mass fraction	$\frac{n_i \cdot M_i}{\sum n_i \cdot M_i}$
$C_p$	specific heat capacity	$\left[\frac{J}{kg \cdot K}\right]$
$k$	thermal conductivity	$\left[\frac{W}{m \cdot K}\right]$

In the model, the dynamic viscosity of the mixture,  $\mu$ , is obtained using the Chapman-Enskog theory. This theory merges the equations of hydrodynamics with the Boltzmann equation, and it describes viscosity in terms of molecular parameters.

$$\mu = \sum_i \frac{\mu_i}{1 + \frac{1}{x_i} \sum_{j,j \neq i} x_j \Phi_{ij}} \quad (4.5)$$

$$\Phi_{i,j} = \frac{(1 + (\mu_i/\mu_j)^{0.5}(M_j/M_i)^{0.25})^2}{(4/\sqrt{2})(1 + M_i/M_j)^{0.5}} \quad (4.6)$$

$$\mu_i = 2.669 \cdot 10^{-6} \frac{\sqrt{TM_j \cdot 10^3}}{\sigma_j^2 \Omega_D} \quad (4.7)$$

$$\Omega_D = \frac{b_1}{(T^*)^{b_2}} + \frac{b_3}{\exp(b_4 T^*)} + \frac{b_5}{\exp(b_6 T^*)} + \frac{4.998 \cdot 10^{-40} \mu_{Di}^4}{k_b^2 T^* \sigma_i^6} \quad (4.8)$$

In the equations above,  $\sigma_j, \epsilon_j$  are the Lennard-Jones potential parameters and  $\Omega_D$  is a dimensionless function of the temperature.

TABLE VI: PARAMETERS OF DYNAMIC VISCOSITY

$\mu$	dynamic viscosity	$[Pa \cdot s]$
$\sigma_j$	L-J potential parameter	$[\text{\AA}]$
$\epsilon_j$	L-J potential parameter	$[J]$
$k_b$	Boltzmann constant	$[\frac{J}{K}]$
$T^*$	dimensionless temperature	$\frac{T \cdot k_b}{\epsilon_j}$

TABLE VII: VALUES OF  $b$  OBTAINED BY GARG AND ACHARI [38]

$b_1$	1.16145	[-]
$b_2$	0.14874	[-]
$b_3$	0.52487	[-]
$b_4$	0.77320	[-]
$b_5$	2.16178	[-]
$b_6$	2.43787	[-]

The diffusivity of the gas is evaluated by the Maxwell-Stefan diffusivity formula. Since the problem analyzed is one-dimensional, in the divergence  $\nabla$ , only by the term in the axial direction,  $\frac{d}{dz}$ , is present.

$$\frac{d}{dz} \left[ -\rho\omega_i \sum_j D_{ij} \left[ \frac{M}{M_j} \left( \frac{d\omega_j}{dz} + \omega_j \frac{dM}{dz} \frac{1}{M} \right) + (x_j - \omega_j) \frac{dP}{dz} \frac{1}{P} \right] + \omega_i \rho u \right] = r_i \quad (4.9)$$

$$D_{ij} = D_{ij}^0(T_0, P_0) \frac{P}{P_0} \left( \frac{T}{T_0} \right)^{1.5} \quad (4.10)$$

In Eq. (4.10),  $D_{ij}^0$  is the binary diffusion coefficient [ $\frac{m^2}{s}$ ] obtained from empirical correlations. For the present case, the gas flows through a porous matrix, therefore the effective binary diffusivity is corrected with the Millington and Quirk correlation, Eq. (4.11).

$$D_{ij,eff} = D_{ij}\phi^{\frac{4}{3}} \quad (4.11)$$

When considering the mass balance, Eq. (4.12), it should be noted that the number of moles of species changes due to carbon dioxide hydrogenation.

$$\frac{d}{dz}j_i + \rho \left( \frac{du}{dz} \right) \omega_i = r_i \quad (4.12)$$

In the mass balance, the term  $\mathbf{j}_i$  considers the diffusivity of the gasses. The driver of this motion can be a mass fraction difference or a temperature gradient.

$$j_i = - \left( \rho D_i^m \frac{d\omega_i}{dz} + \rho \omega_i D_i^m \frac{dM_n}{dz} \frac{1}{M_n} - \mathbf{j}_{e,i} + D_{e,i}^T \cdot \phi^{\frac{4}{3}} \frac{dT}{dz} \frac{1}{T} \right) \quad (4.13)$$

TABLE VIII: PARAMETERS OF THE MASS BALANCE EQUATION

$D_i^T$	thermal diffusion coefficient	$\left[ \frac{kg}{m \cdot s} \right]$
$D_i^m$	$\frac{1-\omega_i}{\sum_{k \neq i} \frac{x_k}{D_{ik,eff}}}$	$\left[ \frac{m^2}{s} \right]$
$M_n$	$\left( \sum_i \frac{\omega_i}{M_i} \right)^{-1}$	$\left[ \frac{kg}{mol} \right]$
$j_{c,i}$	$\rho \omega_i \sum_k \frac{M_i}{M_n} D_k^m \frac{dx_k}{dz}$	$\left[ \frac{kg}{m^2 \cdot s} \right]$
$r$	reaction rate	$\left[ \frac{kg}{s \cdot m^3} \right]$

As the gas mixture flows through the porous matrix, it experiences a pressure drop that can be described by the Ergun equation.

$$\frac{dP}{dz} = -\frac{G}{\rho_{fluid} D_p} \left( \frac{1-\phi}{\phi^3} \right) \left[ \frac{150(1-\phi)\mu}{D_p} + 1.75G \right] \quad (4.14)$$

In the equation above, the parameter  $G$  represents the product of the fluid density and velocity. Eq. (4.14) can be rewritten if the fluid is treated as a mixture of ideal gases, since the density depends on pressure, temperature and quantity of moles.

$$\frac{dP}{dz} = -\frac{G}{\rho_{0,fluid} D_p} \left( \frac{1-\phi}{\phi^3} \right) \left[ \frac{150(1-\phi)\mu}{D_p} + 1.75G \right] \left( \frac{P_0}{P} \right) \left( \frac{T}{T_0} \right) \left( \frac{n_{mol}}{n_{mol,0}} \right) \quad (4.15)$$

In the energy balance, Eq. (4.16), thermal energy is produced and consumed by the chemical reactions, while, at the same time, heat is exchanged with the refrigerant fluid that flows in the shell.

$$(uc_{tot})\bar{c}_p \frac{\partial T}{\partial z} = \rho_{bed} \sum_{j=1} (-r_j \Delta H_j) - \frac{4}{d_{tube}} U'_A (T - T_C) \quad (4.16)$$

In order to determine the overall heat transfer coefficient  $U'_A$ , a series of resistances is considered, which include, conductivity of the metallic tube, and the heat transfer coefficients for heat transfer inside and outside the tube. In the shell, the temperature of the cooling fluid remains constant because the refrigerant fluid absorbs latent heat. This behavior can be approximated as that of molten salt. For the outer boundary coefficient  $\alpha_{out}$ , a value of 7500  $\frac{W}{m^2 \cdot K}$  has been reported [39].

$$\frac{1}{U'_A} = \frac{1}{\alpha_{eff}} + \frac{1}{\alpha_{out}} \quad (4.17)$$

The effective heat transfer coefficient for the inner part of the tube can be approximated, thanks to de Wasch and Froment's model, to a series of two resistances, one that describes the heat transfer near the wall,  $\alpha_W$ , and the other the transport in the reactor and that depends on the radial dispersion coefficient,  $\Lambda_r^{eff}$  [40].

$$\frac{1}{\alpha_{eff}} = \frac{1}{\alpha_W} + \frac{d_{tube}}{8\Lambda_r^{eff}} \quad (4.18)$$

The term  $\Lambda_r^{eff}$  depends on a stagnation term and a dynamic term. The stagnation is proportional to the conductivity of the porous matrix and gas mixture and to the porosity of the bed, while the dynamic part depends on the Peclet number, a dimensionless value that represents the ratio between the advective and the diffusive transport rate.

The heat transfer coefficient that describes the heat transport in the reactor  $\alpha_W$  is obtained from the Nusselt number, described by the empirical correlation of Martin and Nilles [40].

From all the equations reported above, it is possible to understand that both mass and energy balance depend on the kinetic rate of the reactions that, in their turn, depends on temperature and pressure. Therefore, the set of equations is fully coupled and all the equations must be solved at the same time.

#### 4.2.1 Boundary Conditions: 1D Model

In the 1D model of the reactor, all the process is considered to evolve along the axis of the tube. Under this simplification, the geometry studied is a straight line and only two nodes are at the boundary of the domain: the inlet and the outlet. At the inlet, the gaseous stream flows inside the domain with a fixed pressure, temperature and composition. The number of moles that flow each second inside the geometry fixes the velocity. At the outlet, is imposed a no back-flow condition, Eq. (4.19).

$$-\mathbf{n} \cdot \rho D_i^m \nabla \omega_i = 0 \quad (4.19)$$

### 4.2.2 Computational Model: 1D Model

COMSOL solves the mathematical problem by dividing the domain in smaller elements [43]. This generates a mesh that allows to solve the system with a finite element method. The stationary nonlinear solver must consider the equations as fully coupled and it should solve all the unknowns at the same time in every single iteration. Even though this is relatively expensive to do, it will lead to a more robust convergence, compared to the segregated approach, in which different groups of variables are generated and solved independently one from the other.

The nonlinear method used for this specific case is the "automatic Newton", which implements a damped Newton's method approach. This method starts using an initial guess  $U_0$ , and a linearized model is created using  $U_0$  as the linearization point. Then, the solution vector  $U$  is then used to define the residual vector  $f(U) = 0$ . After that, the Jacobian matrix of the residual vector is generated from the first-order partial derivatives, and used to solve the discretized form of the linearized model for the Newton step  $\delta U$  using the selected linear system solver.

$$J(U_0)\delta U = -f(U_0) \quad (4.20)$$

The new iteration is computed using the previous solution and the damping factor  $\lambda$ .

$$U_1 = U_0 + \lambda\delta U \quad 0 \leq \lambda \leq 1 \quad (4.21)$$

At last, the relative error  $E$  for the new iteration is defined, as shown on Eq. (4.22).

$$J(U_0)E = -f(U_1) \quad (4.22)$$

The method reduces  $\lambda$  and computes again  $U_1$  until the new error is smaller than the one of the previous iteration. When this condition is reached, the algorithm proceeds with the next iteration. When the damping factor is equal to 1, the method converges quadratically if the initial guess  $U_0$  is sufficiently close to a solution. The termination criterion used is based on solution convergence. Indeed, the software stops the iterations when the relative tolerance exceeds the relative error as calculated with Eq. (4.23).

$$error = \sqrt{\frac{1}{M}} \sqrt{\sum_{j=1}^M \frac{1}{N_j} \sum_{i=1}^{N_j} \left( \frac{|E_{i,j}|}{W_{i,j}} \right)^2} \quad (4.23)$$

In the equation above,  $M$  represents the number of fields while  $N_j$  the degrees of freedom in a specific field. The parameter  $E_{i,j}$  the estimated error, while  $W_{i,j}$  is the maximum value between the current approximation to the true and the scaling factor  $S_{i,j}$ . The scaling factor, for the automatic Newton method is the average of  $|U_{i,j}|$  solution for all the degrees of freedom of a fixed field, times a factor equal to 0.1. When the automatically damped Newton solver is used, the solver monitors the convergence only if  $\lambda$  for the current iteration is 1. Therefore, even if the estimated error is smaller than the requested relative tolerance, the iteration continues as long as the damping factor is not equal to 1. Within each iteration, a linearized system of equation is solved using the direct solver MUMPS. This solver works on system of the form

$Ax = b$  by performing the LU factorization of the matrix  $A$  and permuting the columns to minimize the number of non-zeros in the  $L$  and  $U$  matrices.

The number of elements into which the domain is subdivided determines how fast the solution will converge: the higher the number, the more computationally expensive the model will be. However, for finer refinements of the mesh, a lower error is generated from the linear approximation of the system. Therefore, it is necessary to find a trade-off for the number of elements used in order to obtain the minimal cost for required accuracy[44]. In order to assess the optimal number of elements, the refinement of the mesh has been varied and the number of elements increased from 3 to 100, value has been varied in a range between 3 to 100, while the rest of the parameters are kept fixed in the model.

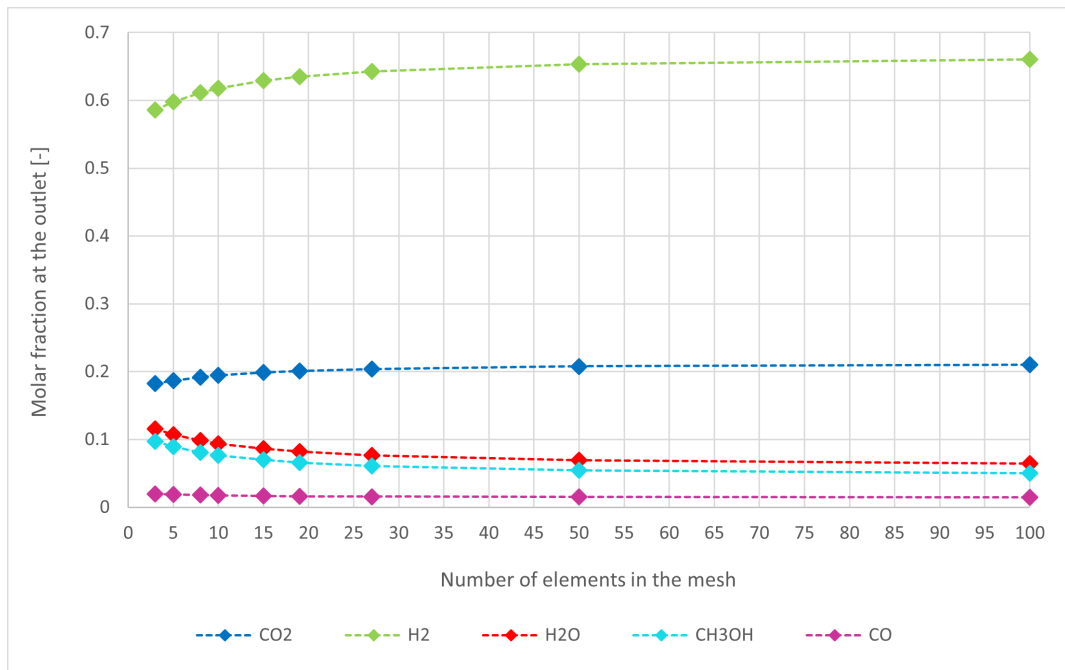


Figure 20: Effect of mesh refinement on outlet mixture composition - 1D

Figure 19 shows the variation of the outlet mixture composition with the number of elements. As indicated, the solution becomes nearly grid independent for the number of elements greater than 27.

### 4.2.3 Results and Validation: 1D Model

As already stated, the model needs to be validated before using its results to assess how the parameters interact with each other and which are the optimal working conditions of the plant. The validation could be performed in different ways: for example, by comparing the data

obtained from the model with data available in literature, or with data from plants operating in the same or similar conditions of the case studied.

Unfortunately, while many data are available for the production of methanol starting from syngas, not a lot of information is freely available regarding the direct thermocatalytic process. For this reason, in this specific case, data obtained in similar conditions are used. Kondarides et al. published an article in 2020, about CO<sub>2</sub> hydrogenation over the catalyst CuO/ZnO/Al<sub>2</sub>O<sub>3</sub>. The experiments reported in their paper were performed at atmospheric pressure and with an inlet stream composition of 10% CO<sub>2</sub> and 90% hydrogen [45], on a catalyst mass of 200 mg and total flow rate of 50  $\frac{cm^3}{min}$ . For the same reactor conditions, the fraction of reacted CO<sub>2</sub> and the methanol yield obtained from the computational model are compared to the experimental data.

The methanol yield is expressed as the ratio of the number of moles of methanol in the outlet stream to the number of moles of carbon dioxide at the inlet, as indicated in Eq. (4.24).

$$Y_{CH_3OH} = \frac{n_{CH_3OH,out}}{n_{CO_2,in}} \quad (4.24)$$

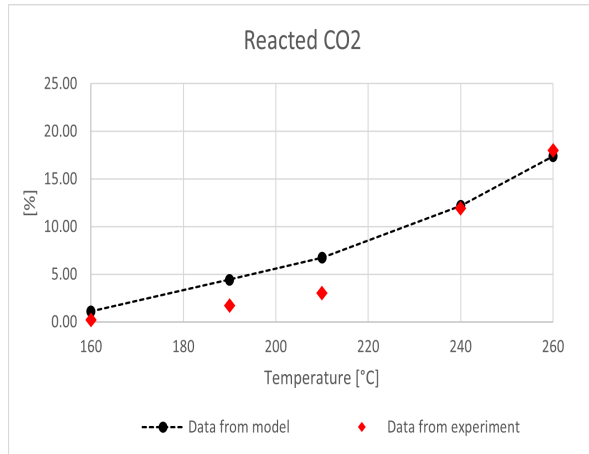
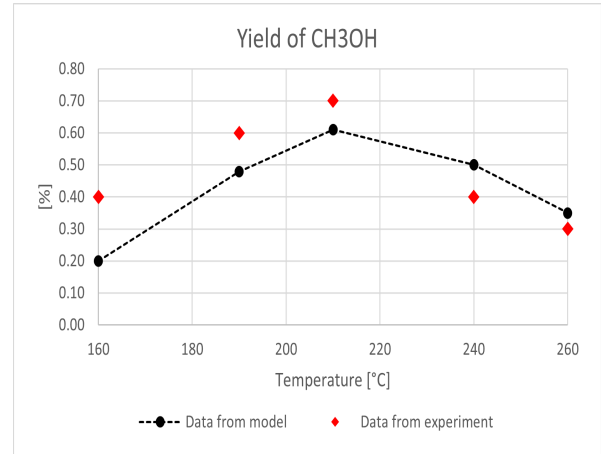
Figure 21: Model validation: reacted CO<sub>2</sub>

Figure 22: Model validation: methanol yield

The pressure at which the experiments were performed is far from 5 MPa, which represents the optimal conditions with respect to methanol yield for the selected catalyst. For this reason, the reaction rate is very low, and only a small fraction of carbon dioxide is consumed, producing a negligible temperature increase. In general, simulations capture the experimental data reasonably well, as indicated in Figs. 20 and 21. There are some discrepancies, which may be due to fact that the model validation has been done at conditions different from the ones at which the reaction kinetics has been developed.

After the validation, the model can be used to observe how the generation of methanol is influenced by different parameters. In order to assess that, the parameters reported in Table VIII are kept fixed in the simulation.

TABLE IX: SHELL AND TUBE REACTOR CHARACTERISTICS

Number of tubes	$n$	200	-
Tubes radius	$r_{tubes}$	0.0362	m
Tube length	$l_{tubes}$	8	m
Volume tubes	$V_{tubes}$	$n \cdot l_{tubes} \cdot \pi \cdot r_{tubes}^2$	$m^3$
Porosity	$\phi$	0.45	-
Catalyst	CuO/ZnO/Al <sub>2</sub> O <sub>3</sub>		
Diameter of the catalyst particles	$D_p$	5	mm
Catalyst density	$\rho_{catalyst}$	1200	$kg/m^3$
Bed density	$\rho_{bed}$	$(1 - \phi)\rho_{catalyst}$	$kg/m^3$
Catalyst mass	$m_{catalyst}$	$\rho_{bed} \cdot V_{tubes}$	$kg$
Inlet flow rate	$Q_{mol,in}$	700	$mol/s$
Weight Hour Space Velocity	$WHSV$	250	$7[h^{-1}]$
Temperature refrigerant fluid	$T_C$	250	$^{\circ}C$

A parameter used to assess the performance of the reactor is the selectivity of the catalyst towards methanol, which is defined as the ratio between the number of moles of CH<sub>3</sub>OH and the sum of CH<sub>3</sub>OH and CO moles at the outlet.

$$selectivity_{CH_3OH} = \frac{n_{CH_3OH,out}}{n_{CH_3OH_2,out} + n_{CO,out}} \quad (4.25)$$

The first parameter that has been changed is the composition of the inflow gas mixture. Pressure and temperature are kept fixed at the inlet of the tube at 5 MPa and 240 °C, respectively. The ratio between the number of moles of H<sub>2</sub> and the moles of CO<sub>2</sub> has been changed in the range between 0 to 9. This range has been selected, keeping in consideration that in literature [36], the most used value is the stoichiometric ratio of 3. Therefore, this parameter has been modified in a range not too far from the original value.

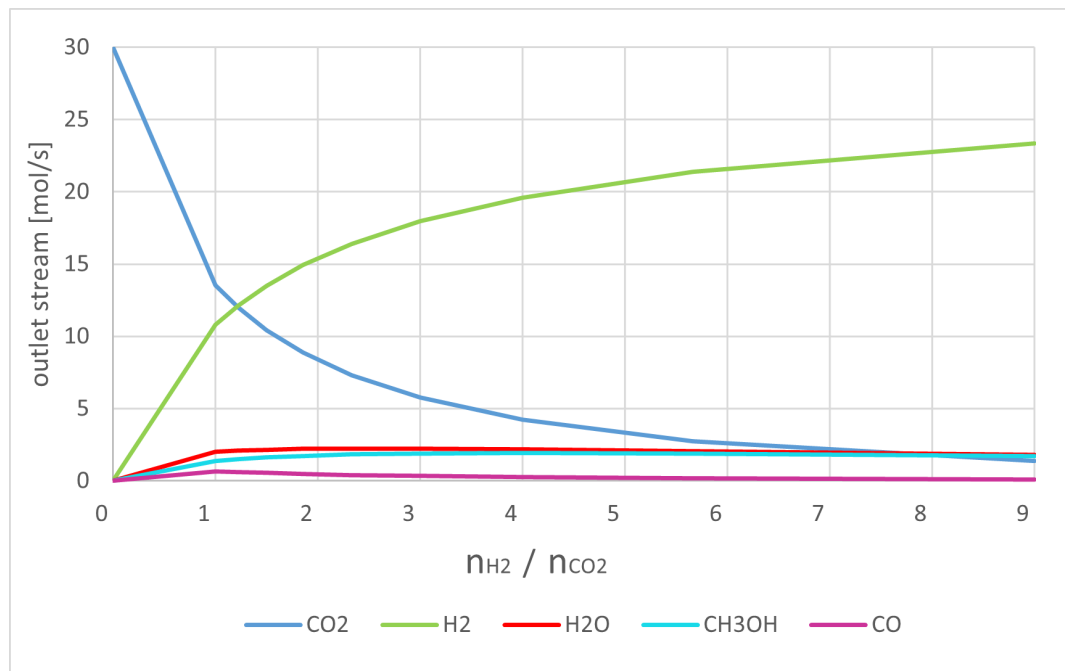


Figure 23: Outlet composition dependence on the inlet composition

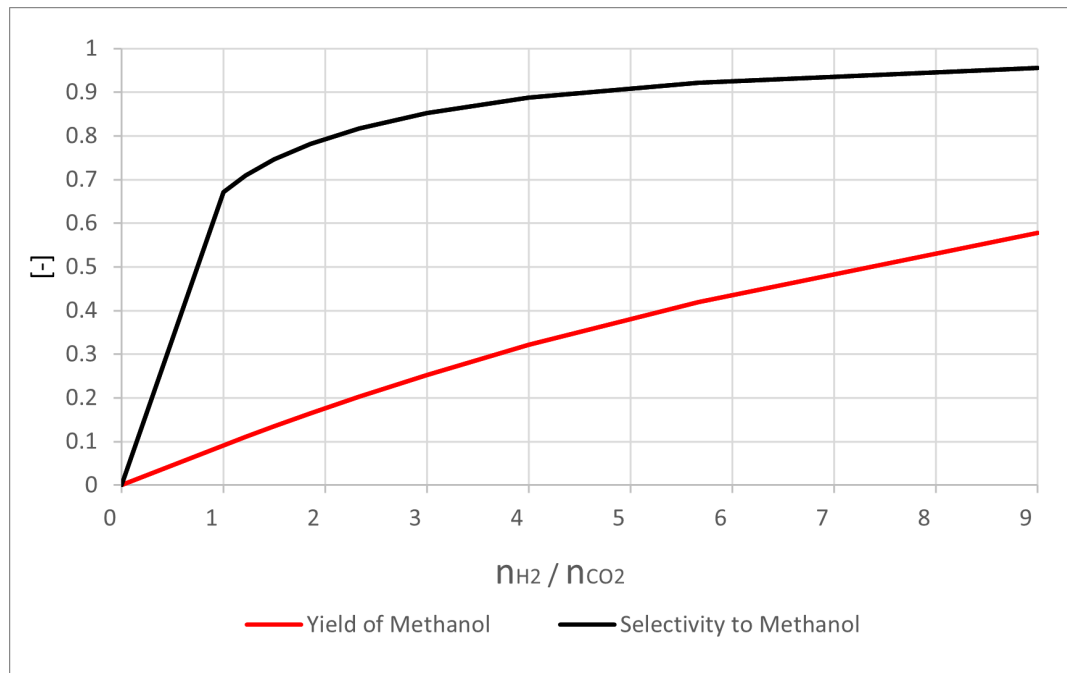


Figure 24: Methanol yield and selectivity dependence on the inlet composition

Both yield and selectivity increase with the increase of the concentration of hydrogen in the mixture; in fact, the smaller number of hydrogen moles favors the reverse water gas shift reaction over the carbon dioxide hydrogenation, which requires more moles of hydrogen per mole of carbon dioxide to react. However, from Fig.23, it is clear that the number of moles of methanol produced per second do not increase significantly with the increase of the relative amount of hydrogen at the inlet. After the ratio equals to 3, the number of moles of methanol at the outlet reaches a plateau. Therefore, this value can be used in the reactor to obtain a

good yield of methanol, and it is possible to avoid requiring an excessive amount of hydrogen from the electrolyzer.

The next parameter analyzed is the change of pressure at the inlet. The change of the pressure in the reactor will modify some properties of the gas and it could change the equilibrium of the reactions. For this reason, its influence in the process has been assessed. The optimal operating condition to produce methanol on this catalyst, are reported in literature [37], to be around 5 MPa. Therefore, the inlet pressure has been changed in a range from 3 to 6 MPa, while the temperature is kept constant at 240 °C and  $\text{H}_2:\text{CO}_2$  is 3.

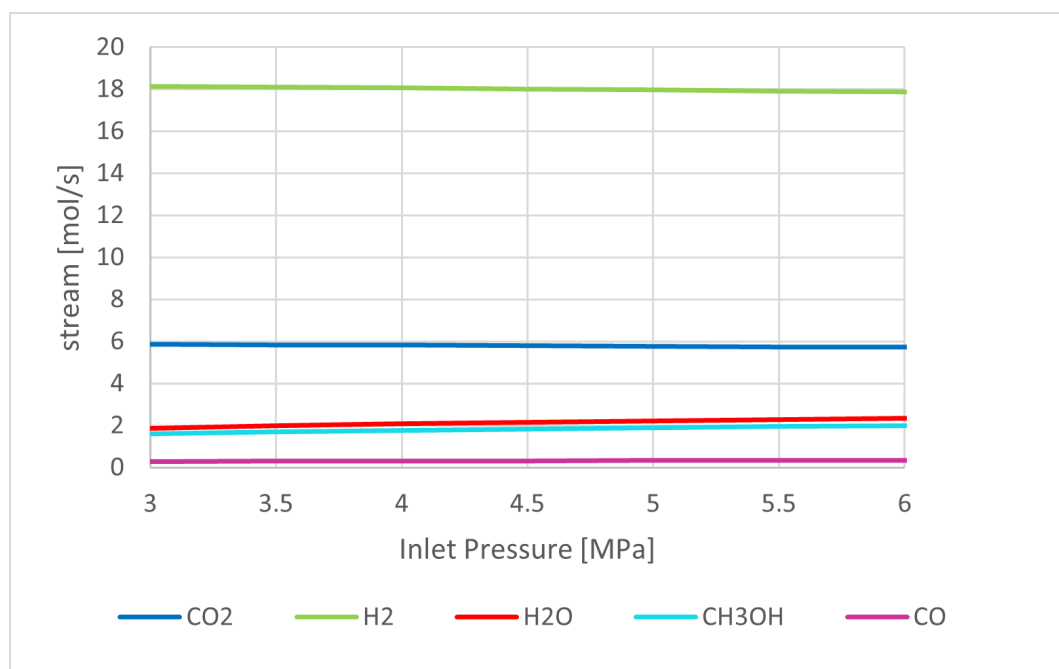


Figure 25: Outlet stream composition dependence on the inlet pressure

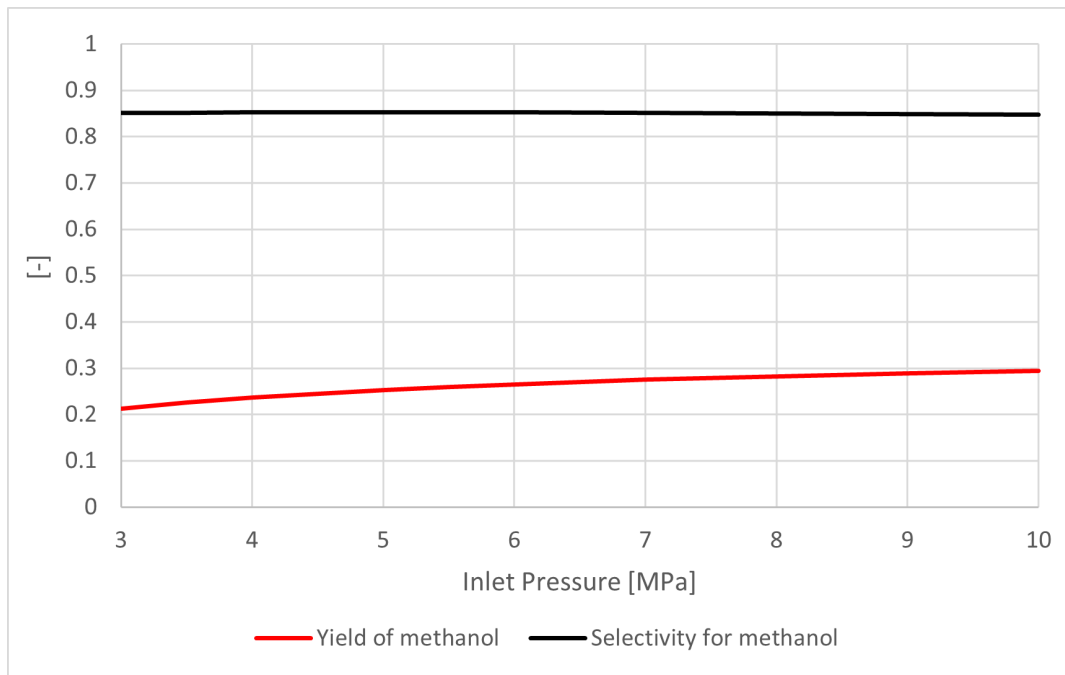


Figure 26: Methanol yield and selectivity dependence on the inlet pressure

An important observation from the figures is that in the pressure range analyzed, the inlet pressure does not influence much the selectivity for methanol. On the other hand, at higher pressure, the methanol yield increases. This is due to the fact that the carbon dioxide hydrogenation evolves from a higher to a lower number of molecules, therefore, according to Le Châtelier principle, is favored at high pressure. Indeed, even if in Fig. 25 the changes in the yield seems negligible, it could be better appreciated in Fig.26, where the scale is smaller.

The last parameter analyzed is the inlet temperature, which is varied in a range between 190 to 290°C, while inflow composition  $H_2:CO_2$  and pressure are kept constant at 3:1 and 5 MPa,

respectively. The upper temperature boundary has been selected to obtain a good conversion of carbon dioxide, but avoiding the risk of deactivation of the catalyst that can occur at relatively high temperatures.

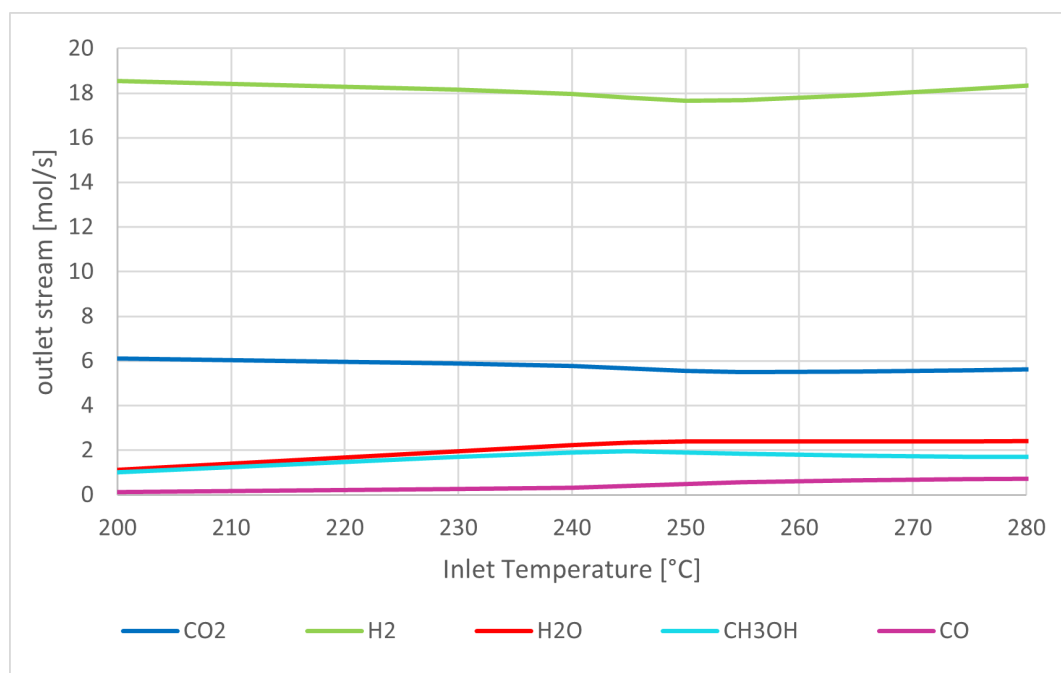


Figure 27: Outlet stream composition dependence on the inlet temperature

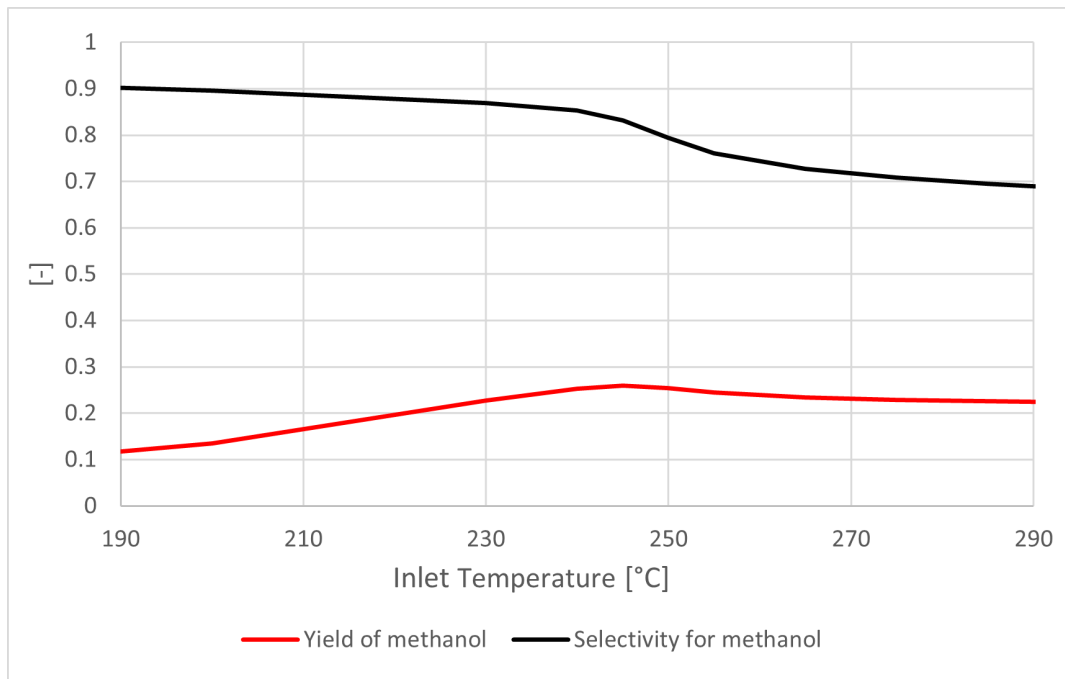


Figure 28: Methanol yield and selectivity dependence on the inlet temperature

The reaction constants depend on the temperature with an Arrhenius-like relationship, however, when the temperature increases, it also increases the production of CO. This generates a particular relationship between temperature and methanol yield that, as shown in Fig. 28, tends to increase up to a certain point and decrease afterwards. The selectivity decreases with the temperature because the endothermic reverse water-gas shift reaction is favored at higher temperature. Also, one may deduce from Figs. 27 and 28 that the optimal inlet temperature is 240 °C.

### 4.3 Two-Dimensional, Pseudo-Homogeneous Reactor Model

The two-dimensional model of the reactor takes into consideration the axial and radial components in the description of the parameters. In this case, the pressure and velocity field depend on two coordinates, and it can be modeled with the help of a build-in physic interface in COMSOL that describes the Brinkmann equations.

$$0 = \nabla \cdot [-P\mathbf{I} + \mathbf{K}] - \left( \mu k^{-1} + \beta \rho |\mathbf{u}| + \frac{Q_m}{\phi^2} \right) \mathbf{u} + \mathbf{F} \quad (4.26)$$

In the equation above,  $Q_m$  is a change in the momentum of the system, while  $\mathbf{I}$  the identity matrix.

$$\nabla \cdot (\rho \mathbf{u}) = Q_m \quad (4.27)$$

$$\mathbf{K} = \mu \frac{1}{\phi} \left( \nabla \mathbf{u} + (\nabla \mathbf{u})^T \right) - \frac{2}{3} \mu \frac{1}{\phi} (\nabla \cdot \mathbf{u}) \mathbf{I} \quad (4.28)$$

In the model presented by Schlereth and Hinrichsen [40], porosity and dispersion coefficients are independent of the radial position. The mass balance is expressed by Eq. (4.29) and the heat balance by Eq. (4.30).

$$\frac{\partial(uc_i)}{\partial z} = \rho_{bed} \sum_{j=1}^{CO2hydr,RWGS} \nu_{i,j} r_j + D_r^{eff} \left( \frac{\partial^2 c_i}{\partial r^2} + \frac{1}{r} \frac{\partial c_i}{\partial r} \right) \quad (4.29)$$

$$(u_{ctot})\bar{c}_p \frac{\partial T}{\partial z} = \rho_{bed} \sum_{j=1}^{CO2hydr,RWGS} r_j(-\Delta_R H_j) + \Lambda_r^{eff} \left( \frac{\partial^2 T}{\partial r^2} + \frac{1}{r} \frac{\partial T}{\partial r} \right) \quad (4.30)$$

The equations are similar to the ones for the 1D case, however, terms are added to each equation to take into account the differences in the radial direction.

#### 4.3.1 Boundary Conditions: 2D Model

The boundary conditions, in this case are more complicated to describe than the one of the one-dimensional model. First of all, on the axis of the tube, the symmetry condition is imposed for all physics. On the external boundary, that represent the external lateral surface of the tube, the no-slip condition is imposed for the flowing fluid. At the inlet of the tube, the condition expressed by Eq. (4.31) is imposed.

$$- \int_{\partial\Omega} (\mathbf{u} \cdot \mathbf{n}) r_{tube} dS = m \quad (4.31)$$

In the equation above,  $m$  is the normal mass flow rate expressed in  $\frac{kg}{s}$ . At the outlet, a pressure condition  $p_0$  of 4.999 MPa and suppressed backflow is imposed.

$$[-P\mathbf{I} + \mathbf{K}] \mathbf{n} = -p_0^* \mathbf{n} \quad (4.32)$$

Where  $p_0^* \leq p_0$ .

For the thermal part of the problem, on the external lateral surface, the heat transfer with the refrigerant fluid at constant temperature is imposed and the heat exchange coefficient considers the thermal resistance of the wall of the tube, and the convection of the cooling water. At the inlet, temperature is determined by the one of the stream entering the tube.

### **4.3.2 2D Computational model**

In the case of the 2D axial-symmetric problem, that analyses also the differences in the radial direction, as in the 1D one, because of the coupling between all the variables in the mathematical model, the fully coupled approach has been used. The non-linear solver uses the automatic highly non-linear Newton method. This algorithm is different from the automatic Newton one because it starts with more damping, therefore it is slower but more likely to converge. The linear solver used is direct MUMPS.

The study of the mesh, in this case, is even more important than in the one-dimensional case, since the number of elements are about three orders of magnitude higher. From Fig.28, it can be assessed that increasing the mesh refinement above 12000 elements is not necessary because the accuracy of the results obtained does not improve significantly after this value, while the computational time, and therefore the cost, increases from 107 seconds, in the case of 11832 elements, to 1235 second for 111414 elements.

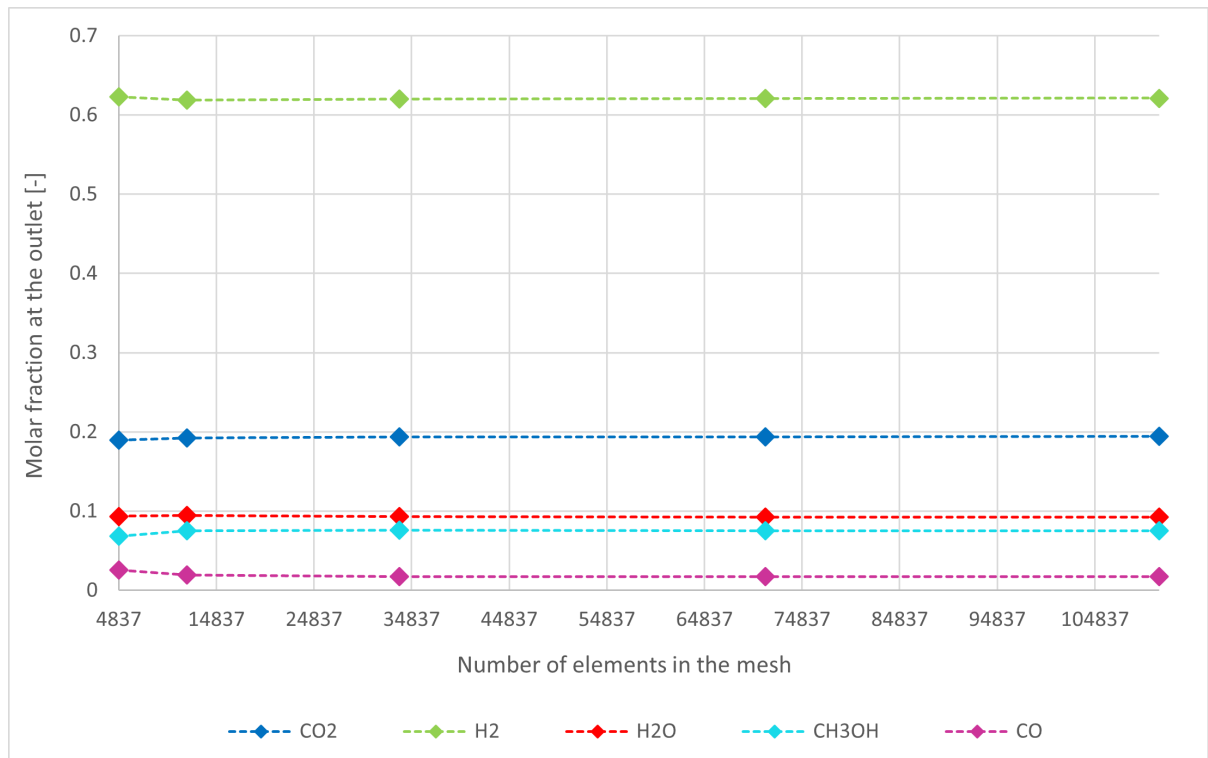


Figure 29: How the mesh refinement affects the result - 2D model

#### 4.4 Results and Comparison between 1D and 2D model

The two models describe the same process, however the 2D axisymmetric approach allows to obtain a full understanding of what happens in the radial direction of the tube. In the analyzed component, due to the no slip condition at the boundary, a velocity gradient is present, as shown in Fig. 29. Indeed, after an initial transient phase, the maximum velocity of the gas is at the center of the geometry, on the axis of symmetry.

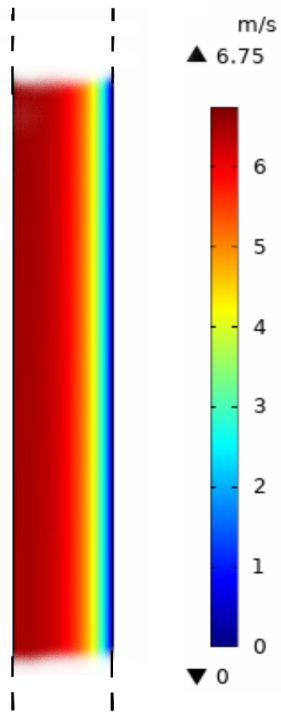


Figure 30: Velocity field

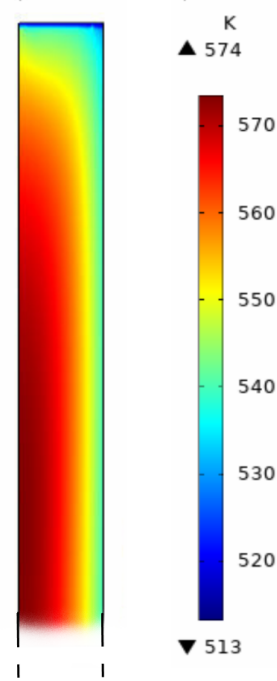


Figure 31: Temperature field

At the external boundary of the tube, the temperature is lower because, on the lateral surface, the tube is in contact with the refrigerant fluid that extracts heat. The higher temperature at the center of the component favors the reverse water-gas shift reaction. For this reason, the molar fraction of CO is higher near the center of the tube compared to its concentration near the external wall.

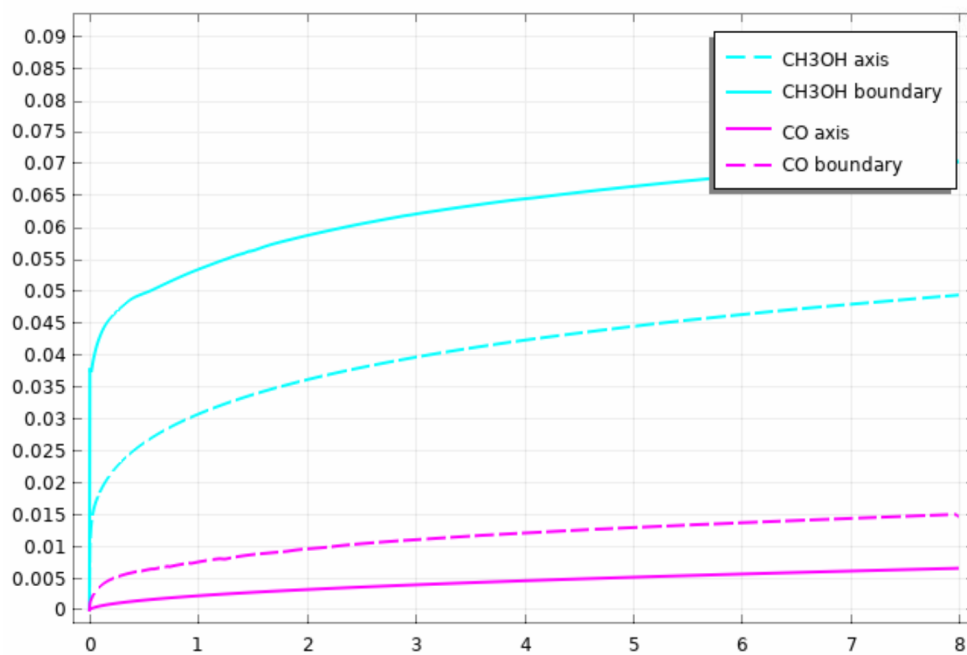


Figure 32: CH<sub>3</sub>OH and CO molar ratio at the axis and the outer boundary

Despite the differences due to the radial component in the model, it is possible to compare the results obtained from the 1D model to the one obtained from 2D one. In order to do so, inflow composition, inlet temperature and pressure have been varied in the ranges discussed above for the 1D model. The methanol yield and selectivity obtained, have been plotted on the same graph with curve obtained previously.

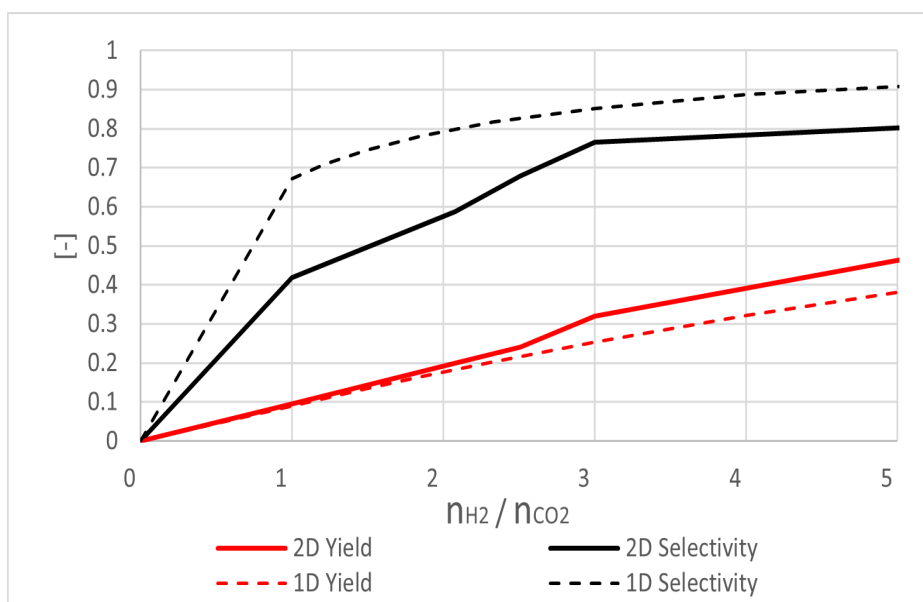


Figure 33: 1D vs 2D dependence on the inlet composition

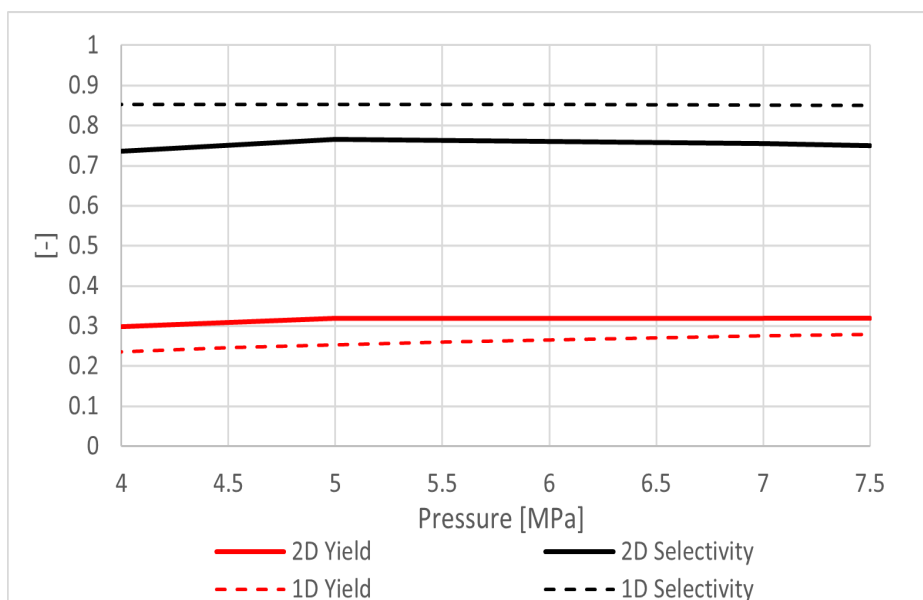


Figure 34: 1D vs 2D dependence on the inlet pressure

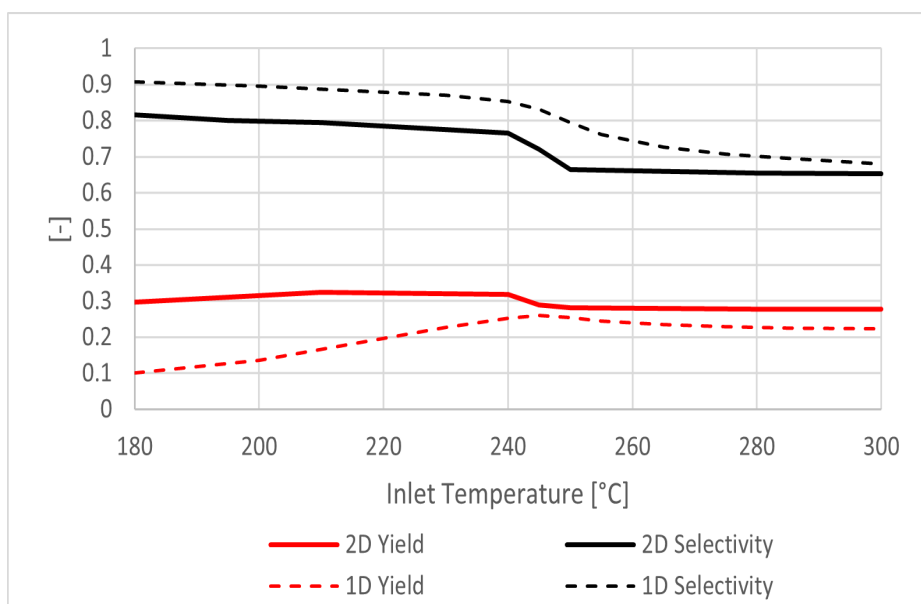


Figure 35: 1D vs 2D dependence on the inlet temperature

In all the cases analyzed, the 2D axisymmetric model yield trends similar to the 1D one; however, the yield is slightly higher, while the selectivity is lower. Even though more carbon dioxide reacts, the lower selectivity could be explained by the velocity and temperature field discussed above.

In conclusion, from both models, it can be assessed that the optimal conditions at which methanol is produced through direct thermocatalytic conversion of  $\text{CO}_2$  are the one reported in Table IX.

TABLE X: OPTIMAL CONDITIONS FOR METHANOL PRODUCTION

H <sub>2</sub> :CO <sub>2</sub> ratio	3	–
Inlet temperature	240	°C
Inlet pressure	5	MPa
Average inlet velocity	2.9471	$\frac{m}{s}$
CH <sub>3</sub> OH yield	30.1	%
CH <sub>3</sub> OH selectivity	81.4	%

Using these values of temperature, pressure and concentration, from the mathematical models, how the molar fraction of the gases change along the axis of the reactor is obtained. In the initial trait of the tube, the kinetic is very fast, and there is significant variation in the composition. But after 5 meters, the amount of products produced increases slowly. However, if the molar flow at the inlet is doubled, both the selectivity and the yield of methanol would decrease, respectively to 77.4 % and 29.7 %. This is due to the higher temperature in the tube.

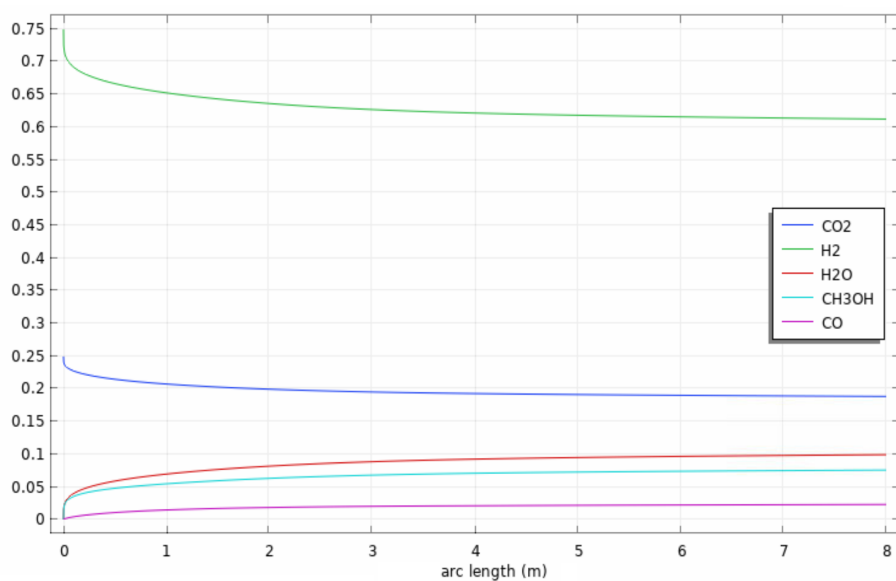


Figure 36: Concentration of the species along the axis of the reactor

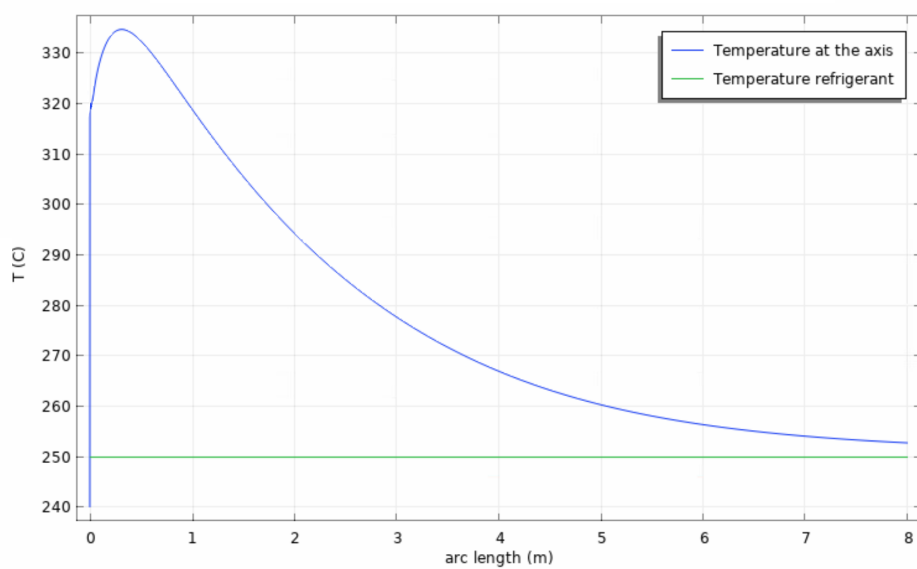


Figure 37: Temperature along the axis of the reactor

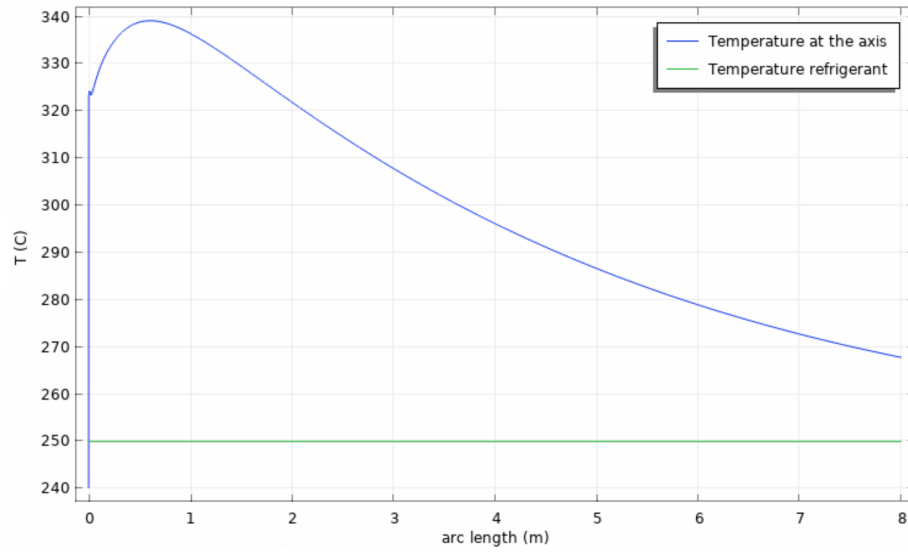


Figure 38: Temperature along the axis of the reactor with doubled inlet flow

## CHAPTER 5

### THERMAL INTEGRATION

When methanol is produced from carbon dioxide through direct thermocatalytic conversion, it is necessary to reduce the energy used in the process to increase the EROI of the fuel. The energy reduction can be achieved through thermal integration of the different parts of the system. In this way, hot streams that need to be cooled down exchange thermal energy with a cold stream that needs to be heat up.

This solution, while reducing the overall energy consumption of the system, is not a straightforward methodology for reducing the overall cost of the plant. Indeed, the installation of additional heat exchangers will increase the initial capital cost while reducing the operational costs. For these reasons, after a first analysis, based exclusively on energy integration, a thermo-economical analysis should be performed in order to assess the best trade-off value of thermal integration. Such value should consider both energy and cost savings, so that the methanol produced will generate the highest revenue possible for the investors. For an analysis based only on energy savings, different approaches could be used to determine the best heat-exchanger network; one of the easiest methods is "Pinch Analysis".

## 5.1 Pinch Analysis

Pinch Analysis is a methodology that provides a systematic approach to determine the maximum energy saving that could be achieved in processes. This methodology is based on mass and energy balances and thermodynamic principles. After these balances are determined, targets for energy saving can be set prior to the design of the heat exchanger network, such as the minimum temperature difference between the hot and cold streams.

In Pinch Analysis, the “Composite Curves” are used to evaluate the biggest achievable energy saving. These curves are the temperature-enthalpy (T-H) profiles of the hot streams and the cold streams in the overall plant. The two curves are plotted in the same graph, in counter-current and, after selecting the minimum temperature difference between the two, they are used to graphically visualize the minimum energy requirement for the process. This is achieved by translating one of the two curves along the horizontal axis, until the minimum temperature condition is verified for each point of the graph. The region of the graph where, if collapsed on the enthalpy axis, the two curves overlap represents the possible energy integration in the system. The point where the two curves approach each other with the minimum temperature difference, takes the name of “Pinch Point”. This point virtually separates the system in part above and in part below the said point. The part above needs to be heated up, for this reason it represents a net heat sink, while the part below, represents a net heat source.

The methodology allows to easily determine the minimum external heating and cooling loads needed in the plant. However, as already stated, when this methodology is applied it could result in an increase in the cost of the final product. For this reason, the minimum

temperature difference selected in the design process, should be determined with particular care. If the minimum temperature difference is too large, the energy recovered in the plant will be low, however, reducing this difference leads to larger areas of heat exchangers and higher costs. Therefore, for a more accurate analysis, energy and cost saving should be considered at the same time in order to select the optimal minimum difference between the streams.

After the parameters' assessment, the possible energy recovery is determined. Then, assuming a counter current scheme of the heat exchangers, it is possible to determine the minimum total surface area, therefore the cost.

## **5.2 Main Thermal Streams in the Process**

In the case studied, three identical reactors, that work in parallel, are used. Each component has the characteristics described in Table IX and works at the conditions reported in Table X. As evaluated by the mathematical models, not all CO<sub>2</sub> and H<sub>2</sub> react. The non-reacted CO<sub>2</sub> and H<sub>2</sub> are extremely precious; therefore, they are separated from methanol and water and recirculated in the process. The recycling of these gases strongly reduces their net production needs and, as a consequence, the energy and costs in the plant will be reduced and the EROI of the fuel improved.

TABLE XI: NET CO<sub>2</sub> AND H<sub>2</sub> NEEDS

	Total inlet [ $\frac{mol}{s}$ ]	Recirculated [ $\frac{mol}{s}$ ]	Net [ $\frac{mol}{s}$ ]
CO <sub>2</sub>	525	398.34	126.66
H <sub>2</sub>	1575	1274.7	300.3
Tot	2100	1673.04	426.96

When the major thermal streams in the plant are analyzed, particular care must be taken in the study of carbon capture, since it is one of the most energy intensive parts in the process. Indeed, the power required for the stripping of the solvent represents the largest thermal energy demand in the plant. This concept has been already introduced in Chapter 2, and a possible solution has been proposed. In fact, substituting the pure monoethylamine solvent with a solution of monoethylamine and ionic liquid, decreases the energy consumption up to 27 %.

TABLE XII: ENERGY NEEDS FOR STRIPPING

Code	Solvent	Energy per $kg_{CO_2}$ $\left[\frac{kWh}{kg_{CO_2}}\right]$	Treated $CO_2$ $\left[\frac{mol_{CO_2}}{s}\right]$	<b>Total Power</b> [kW]	Temperature [°C]
MEA	7m MEA	1.33	126.66	<b>26683.5</b>	120
ILB	Ionic liquid blend	0.97	126.66	<b>19461.02</b>	140

After the desorption,  $CO_2$  flows out from the component at around 110 °C and 2 bar [46]. Now, the gas must reach the operating condition of the reactor of 5 MPa and 240 °C. This can be condition is achieved through a series of compressors and a heat exchanger. The compression is assumed adiabatic and the gas behaving as an ideal gas.

TABLE XIII: CHARACTERISTIC OF THE  $CO_2$  COMPRESSOR

Component	Type	$\eta_c$	Gas	$m\dot{CO}_2$ $\left[\frac{mol_{CO_2}}{s}\right]$	$\gamma_{CO_2}$	$c_{p,CO_2}$ $\left[\frac{kJ}{kgK}\right]$
Compressor	Centrifugal	0.75	$CO_2$	126.66	1.28	0.91

From the reversible adiabatic compression, Eq. (5.1), it is possible to determine the power required for compression and the temperature of the gas at the outlet of the component. In order to avoid an excessive temperature increase, the compression is divided into two steps, separated by an inter-cooler.

$$T_{out,R} = T_{in} \cdot \left( \frac{p_{in}}{p_{out}} \right)^{\left( \frac{1-\gamma}{\gamma} \right)} \quad (5.1)$$

$$W = \frac{n \cdot c_p \cdot (T_{out,R} - T_{in})}{\eta_c} \quad (5.2)$$

$$T_{out} = T_{in} + \frac{W}{n \cdot c_p} \quad (5.3)$$

TABLE XIV: ENERGY NEEDS FOR THE COMPRESSION OF CO<sub>2</sub>

Code	Stage	Inlet P [bar]	Outlet P [bar]	Inlet T [K]	Outlet T [K]	Power [kW]
CC1	I Compressor	2	18	383.15	698.41	160.02
HXC1	I Heat Exchanger	18	18	698.41	413.15	<b>-1446.72</b>
CC2	II Compressor	18	50	413.15	551.10	699.63
HXC2	II Heat Exchanger	50	50	551.10	513.15	<b>-192.46</b>

At the same time, H<sub>2</sub> also needs to be brought to the temperature and pressure conditions required by the reactor. This gas exits the low temperature alkaline electrolyzer at 80 °C and 3 MPa.

TABLE XV: CHARACTERISTIC OF THE H<sub>2</sub> COMPRESSOR

Component	Type	$\eta_c$	Gas	$\dot{m}_{H_2}$ [ $\frac{mol_{H_2}}{s}$ ]	$\gamma_{H_2}$	$c_{p,CO_2}$ [ $\frac{kJ}{kgK}$ ]
Compressor	Centrifugal	0.75	H <sub>2</sub>	300.3	1.4	14.5

TABLE XVI: ENERGY NEEDS FOR THE COMPRESSION OF H<sub>2</sub>

Code	Stage	Inlet P [bar]	Outlet P [bar]	Inlet T [K]	Outlet T [K]	Power [kW]
CH1	Compressor	10	50	353.15	743.3	3395.09
HXH1	Heat Exchanger	50	50	743.3	513.15	- <b>2002.3</b>

When both CO<sub>2</sub> and H<sub>2</sub> are at 5 MPa and 240°C, they are mixed with the recirculated gases, before entering the reactors.

In the reactors, the chemical transformations generate heat that is removed from the refrigerant fluid that flows in the outer shell. From the mathematical model and the computational results, the amount of heat extracted from each tube is determined.

TABLE XVII: ENERGY EXTRACTED FROM THE REACTORS

Code	Number of tubes	Number of reactors	Power per tube [ $\frac{kW}{tube}$ ]	<b>Power</b> [kW]
REA	200	3	14.86	<b>9680.54</b>

At the outlet of the reactor, the average temperature of the gases is 523.92 K. For this reason, the products must be cooled down before entering the separation columns. Then, the non reacted gases are separated from the liquid methanol and water in the first separation column, at 10 bar and 45 °C. Knowing the composition of the stream from to the computational model described in Chapter 4, it is possible to determine the molar mass and heat capacity of the mix at the outlet. To reach the temperature of 45 °C, the stream is cooled down in an heat exchanger.

TABLE XVIII: ENERGY SUBTRACTED FROM THE PRODUCTS

Code	Molar stream $[\frac{mol}{s}]$	Molar mass $[\frac{kg}{mol}]$	$c_{p,mix}$ $[\frac{kJ}{kg \cdot K}]$	Inlet T [K]	Outlet T [K]	Power [kW]
AFR	2052.17	0.01686	1.561	523.92	318.15	<b>-11115.9</b>

After their separation, CO<sub>2</sub> and H<sub>2</sub> must be brought back to the operation condition of the reactors. The same approach described above, Eq. (5.1) to (5.3), is followed.

TABLE XIX: COMPRESSORS FOR THE RECIRCULATED GASES

Component	Type	$\eta_c$	Gas	$\dot{m}$ $[\frac{mol}{s}]$	$\gamma$	$c_p$ $[\frac{kJ}{kgK}]$
Compressor	Centrifugal	0.75	CO <sub>2</sub>	398.34	1.28	0.91
Compressor	Centrifugal	0.75	H <sub>2</sub>	1274.7	1.4	14.5

TABLE XX: ENERGY NEEDS FOR COMPRESSION OF RECIRC. GASES

Code	Stage	Inlet P [bar]	Outlet P [bar]	Inlet T [K]	Outlet T [K]	Power [kW]
CC3	CO <sub>2</sub> Compressor	10	50	318.15	497.16	2855.13
HXC3	CO <sub>2</sub> Heat Exchanger	50	50	497.16	513.15	<b>+ 255.03</b>
CH2	H <sub>2</sub> Compressor	10	50	318.15	669.63	12717.7
HXH2	H <sub>2</sub> Heat Exchanger	50	50	669.63	513.15	<b>-5661.96</b>

In conclusion, the major thermal streams are summarized in Table XXI. Initially, the case where the solvent used in the absorber is the solution of pure MEA is analyzed.

TABLE XXI: MAIN THERMAL STREAMS

Code	C [ $\frac{kW}{K}$ ]	Inlet T [K]	Outlet T [K]	Power [kW]
MEA	26683.5	393.15	393.14	<b>+26683.5</b>
REA	9680.54	523.15	523.15	<b>-9680.54</b>
HXC1	5.07	698.41	413.15	<b>-1446.72</b>
HXC2	5.07	551.1	513.15	<b>-192.46</b>
HXH1	8.70	743.3	513.15	<b>-2002.3</b>
AFR	54.02	523.92	394.14	<b>-11115.9</b>
HXC3	15.95	497.16	513.15	<b>+255.03</b>
HXH2	36.18	669.63	394.14	<b>-5661.96</b>

With these data the Composite Curves are built. In order to do so, the streams are separated in hot and cold and they are sorted in ascending order of temperature. For every temperature range, the total heating or cooling power need is plotted, creating a piece-wise composite line. When latent heat is exchanged, a small fictitious  $\Delta T$  equal to 1 K is assumed.

TABLE XXII: COLD COMPOSITE  
CURVE

T [K]	C [ $\frac{kW}{K}$ ]	Power [kW]
393.15	266683.5	266683.5
394.15	0	0
497.16	15.95	255.03
513.15		

TABLE XXIII: HOT COMPOSITE  
CURVE

T [K]	C [ $\frac{kW}{K}$ ]	Power [kW]
318.15	54.02	5131.99
413.15	59.09	5909.26
513.15	109.05	981.42
523.15	9798.59	9798.59
523.92	109.05	83.97
551.1	55.03	628.61
669.63	49.95	5921.15
698.41	13.77	396.34
743.3	8.70	390.542

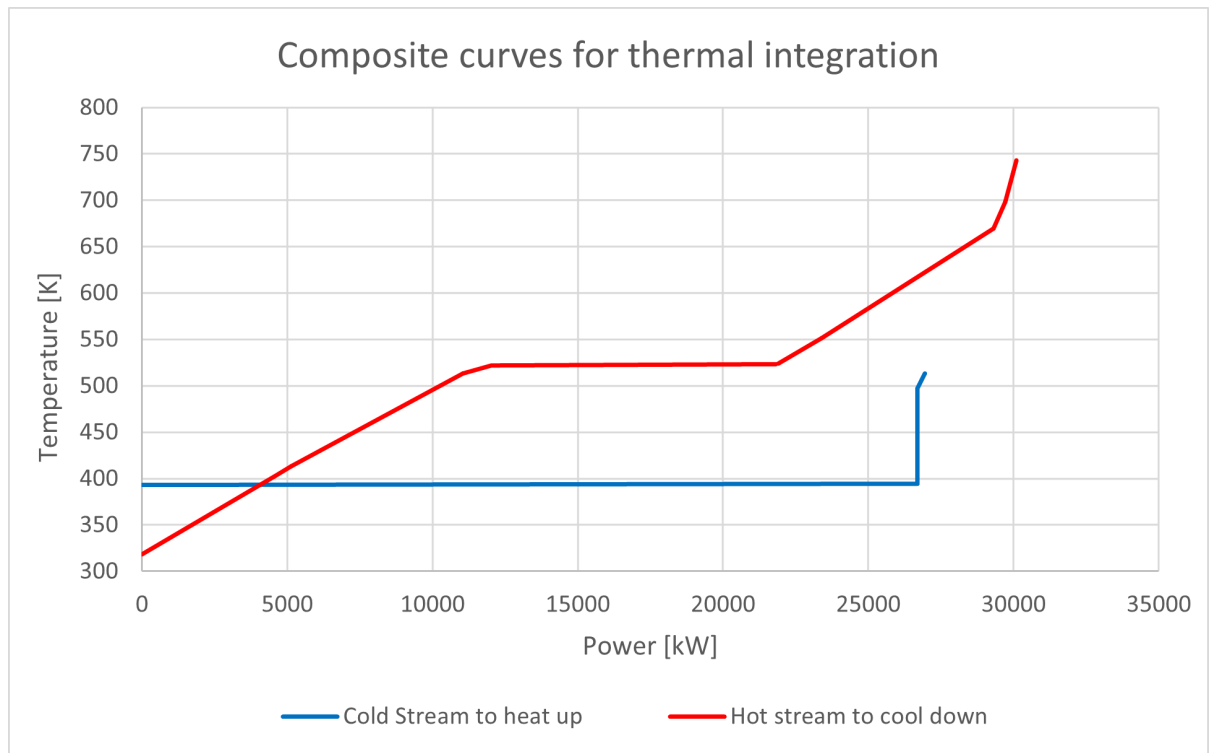


Figure 39: Composite curves thermal integration - case of pure MEA

Then, the minimum temperature difference of 10 K is imposed. To meet this target, the cold composite curve is translated along the horizontal axis, as shown in Fig. 39.

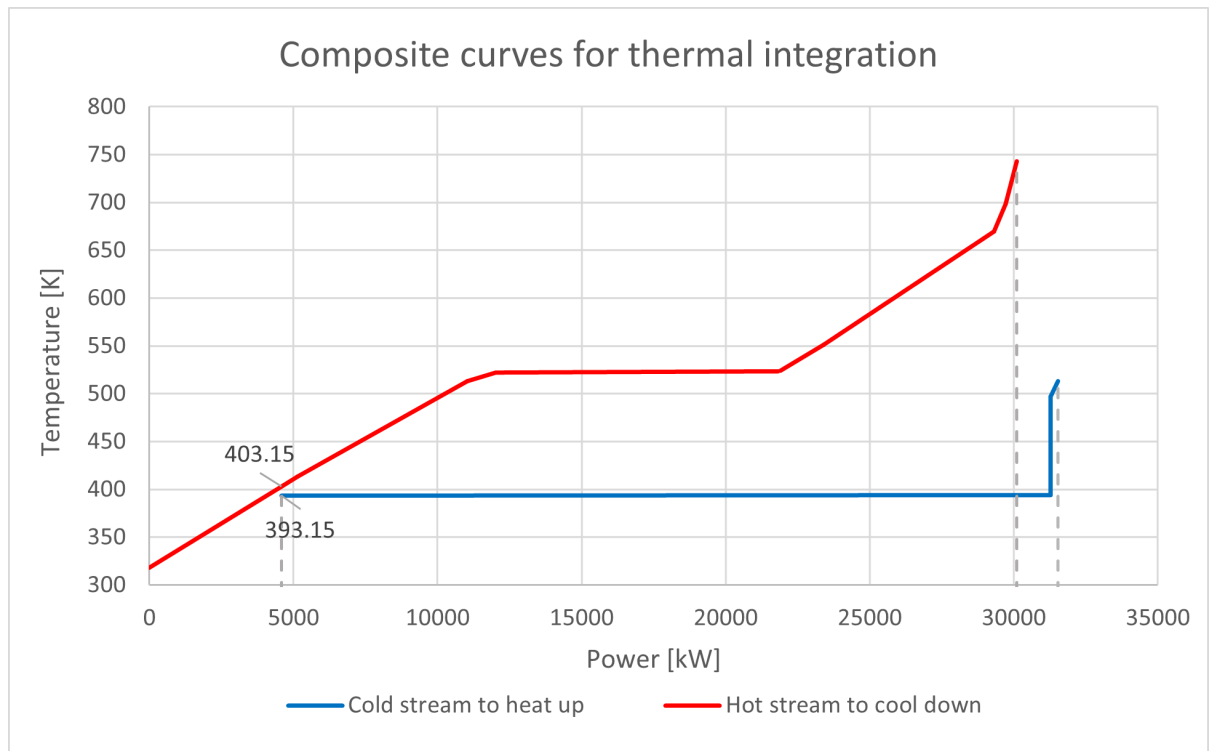


Figure 40: Composite curves thermal integration -  $\Delta T=10$  K

From Figure 40, one may deduce that all the thermal integration takes place above the pinch point, which is at the temperature of 398.15 K, and the maximum heat recovery possible.

TABLE XXIV: THERMAL LOADS AND INTEGRATION - PURE MEA PLANT

	Heat recovery [kW]	Heat needs [kW]	Heat waste [kW]	Saved power needs [%]	Saved power waste [%]
No Integration	0	26938.53	30099.88	0	0
Max Integration	20058.17	1439.35	4591.78	94.6	84.74

The maximum thermal integration possible in the plant reduces the thermal needs by more than 94 %. However, the minimum temperature difference selected in this case is relatively small; therefore, it leads to high surface of heat exchange and high cost. The use of bigger  $\Delta T$  will reduce the amount of heat recovered in the plant, however, it could lead to cost savings.

TABLE XXV: INTEGRATION FOR DIFFERENT  $\Delta T$  - PURE MEA PLANT

$\Delta T$ [K]	Heat recovery [kW]	Heat needs [kW]	Heat waste [kW]	Saved power needs [%]	Saved power waste [%]
10 K	25508.18	1439.35	4591.78	94.6	84.74
30 K	24427.68	2510.85	5672.20	90.68	81.15
50 K	23347.26	3591.27	6752.62	86.67	77.56
100 K	20646.21	6292.324	9453.67	76.64	68.59

Finally, the case of blending of ionic liquid and monoethylamine solvent has been analyzed, and the same procedure described above has been followed. With a minimum temperature difference of 10 K, the pinch point is at 418.15 K. In this case, the minimum  $\Delta T$  could be increased up to 89 K, without compromising the thermal integration.

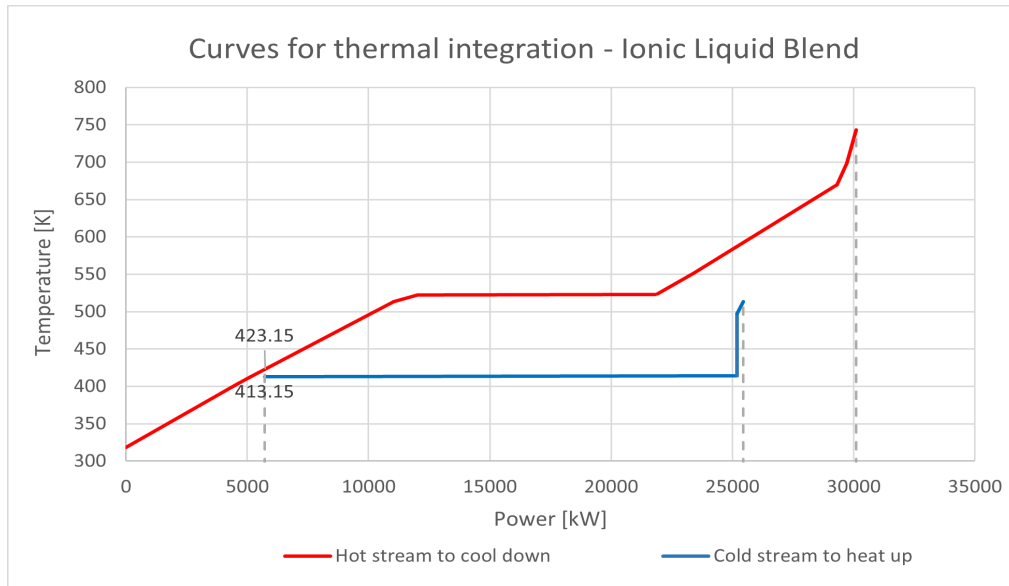


Figure 41: Composite curves thermal integration - ILB plant,  $\Delta T=10K$

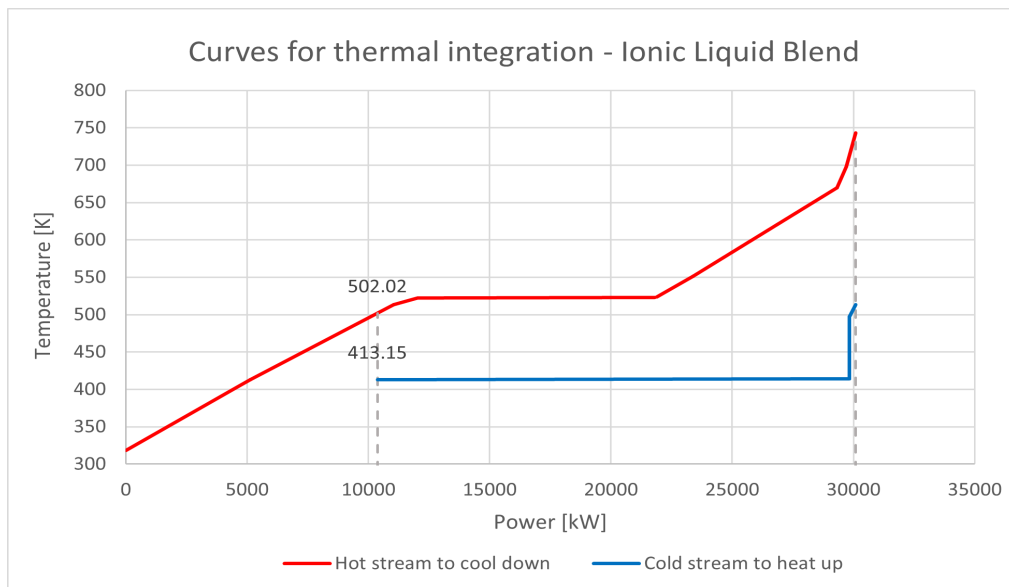


Figure 42: Composite curves thermal integration - ILB plant,  $\Delta T=89K$

TABLE XXVI: THERMAL INTEGRATION - ILB PLANT

$\Delta T$ [K]	Heat recovery [kW]	Heat needs [kW]	Heat waste [kW]	Saved power needs [%]	Saved power waste [%]
No Integration	0	19716.05	30099.88	0	0
10 K	19716.05	0	10383.83	100	65.50
89 K	19716.05	0	10383.83	100	65.50

As shown in Figure 42, increasing the minimum temperature difference up to 89 K will not reduce the share of recovered heat. Using this  $\Delta T$ , the area of heat exchange is reduced, and the costs are decreased. When the ionic liquid blend is used in the carbon capture section, all the heat required in the system could be supplied by the hot streams in the plant that need to be cooled down.

Even though, from this analysis, the ionic liquid blend seems to be the best option, the CO<sub>2</sub> captured with this solvent costs around 150 \$ per tons, three times more than the one captured using pure MEA [47]. For this reason, a thermo-economic analysis of the plant should be performed before assessing which one of the two solvents is more convenient in this process.

### 5.3 Design of the Heat Exchangers' Network

With the streams reported in Table XXI, it is possible to design a network of heat exchangers for thermal integration. In this case, the plant analyzed is the one that works with pure MEA and the minimum temperature difference, between cold and hot streams, is set to 10 K. Initially, the results for thermal integration obtained graphically, using the Composite Curves, are validated by the following procedure: the inlet and outlet temperature of the cold streams are increased by 5 K, while, the temperatures of the hot ones, are decreased by 5 K. These values are reported in Table XXVII, along with the thermal capacity of the stream.

TABLE XXVII: THERMAL STREAMS - PURE MEA PLANT

Code	Type	$T_{in}$ [K]	$T_{out}$ [K]	$T_{in}^*$ [K]	$T_{out}^*$ [K]	C [ $\frac{kW}{K}$ ]
MEA	Cold	393.15	394.15	398.15	399.15	-26683.5
REA	Hot	523.15	522.15	517.15	518.15	9689.54
HXC1	Hot	698.41	413.15	693.41	408.15	5.07
HXC2	Hot	551.1	513.15	546.15	508.15	5.07
HXH1	Hot	743.3	513.15	738.3	508.15	8.70
AFR	Hot	523.92	318.15	518.92	313.15	54.02
HXC3	Cold	497.16	513.15	502.16	518.15	-15.95
HXH2	Hot	669.63	513.15	664.63	508.15	36.18

Now, the streams are sorted in descending order of temperatures and, for every range, the net power is determined, using the global thermal capacity of that specific interval. Then, the net power calculated in the first interval is summed to the value in the second and so on, until the last one. Where the sum reaches the lowest value, that number represents the minimum heat load needed in the plant. Finally, summing that value to the others, the minimum cooling load is obtained. This methodology validates the results obtained graphically.

With these data, a schematic heat exchangers' network is built. This network clarifies how to connect the streams and, eventually, determines the size and operating temperature of every heat exchanger. At last, engineers will have an estimate of the cost of these components. This is a foundational step for the thermo-economic analysis of the overall plant, that could be analyzed in more detail in the future.

TABLE XXVIII: PINCH POINT ANALYSIS - PURE MEA PLANT

$T^*$ [K]	Streams	$\sum C$ [kW/K]	Power per interval [kW]	Total power [kW]	Power with integration [kW]
738.3				0	+ 1431.58
	HXH1	8.7	390.54	390.54	1822.123
693.41					
	HXH1+HXC1	13.77	396.30	786.84	2218.42
664.63					
	HXH1+HXC1+HXH2	49.95	5920.57	607.42	8139.00
546.1					
	HXH1+HXC1+HXH2	55.02	1495.44	8202.86	9734.44
	HXC2				
518.19					
	HXH1+HXC1+HXH2	109.04	83.96	8286.82	9718.40
	HXC2+AFR				
518.15					
	HXH1+HXC1+HXH2	9773.63	9773.63	18060.45	19492.03
	HXC2+AFR+REA+ HC3				
517.15					
	HXH1+HXC1+HXH2	93.09	837.81	18898.26	20329.84
	HXC2+AFR+HXC3				
508.15					
	HXC1+AFR+HXC3	43.14	258.41	19156.67	20588.25
502.16					
	HXC1+AFR	59.09	5555.05	24711.72	26143.30
408.15					
	AFR	54.02	486.18	25197.9	26629.48
399.15					
	AFR+MEA	-26629.48	-26629.48	-1431.58	0
398.15					
	AFR	54.02	4591.7	3160.12	4591.70
313.15					

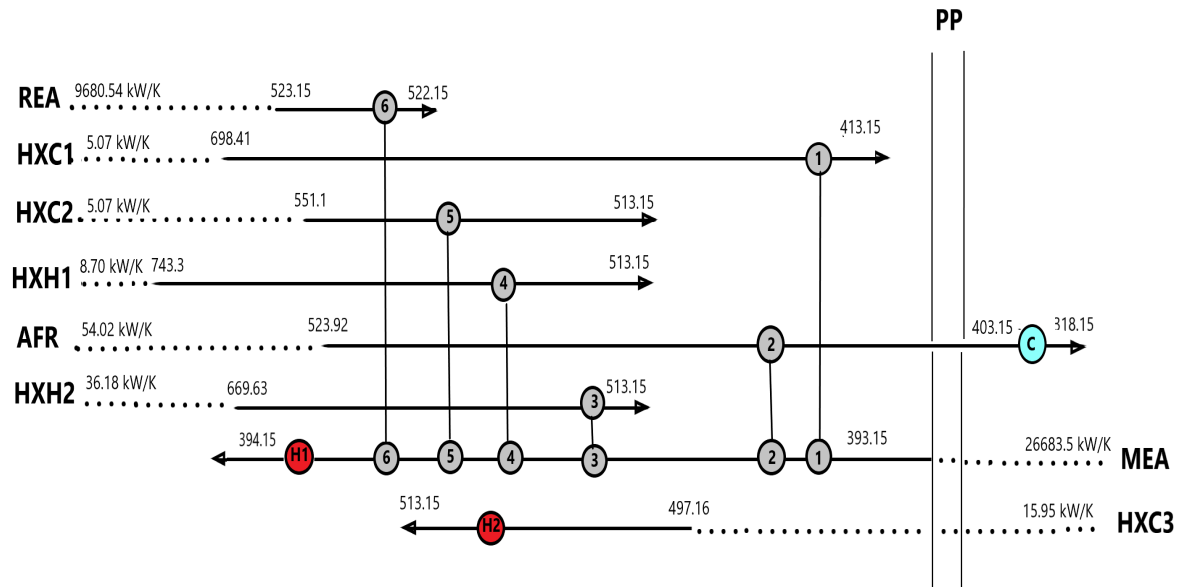


Figure 43: Heat exchangers' network

Some assumptions can be made on the type of heat exchanger and their cost per unit area. In this way the overall cost of the network can be defined. However, it must be stressed that a deeper understanding of the integration should be achieved using a more accurate description of the components of the plant, that can be performed using specific tools, such as Aspen.

TABLE XXIX: HEAT EXCHANGERS' NETWORK - PURE MEA CASE

Component	$T_{HOT,in}$ [K]	$T_{HOT,out}$ [K]	$T_{COLD,in}$ [K]	$T_{COLD,out}$ [K]	Power exchanged [kW]
C	403.15	318.15	EXT	EXT	4591.7
1	698.41	413.15	393.15	393.18	698.41
2	523.92	403.15	393.18	393.42	6524.3
3	669.63	513.15	393.42	393.63	5661.96
4	743.3	513.15	393.42	393.71	2002.3
5	551.1	513.15	393.71	393.71	192.46
6	523.15	522.15	393.71	394.0	9680.54
H1	EXT	EXT	394.0	394.15	4077.85
H2	EXT	EXT	497.16	513.15	255.03

For an heat exchanger of the type double pipe, the cost of the component can be evaluated by Eq. (5.4), where the parameter  $A_{hx}$  is the area of heat exchange [48].

$$C = 10^{(K_1 + K_2 \log A_{hx} + K_3 (\log A)^2)} \quad (5.4)$$

TABLE XXX: PARAMETERS FOR THE COST OF HEAT EXCHANGERS

Component	Type	$K_1$	$K_2$	$K_3$
Heat Exchanger	Double Pipe	3.3444	0.2745	-0.0472

Assuming a counter-current scheme, the area can be evaluated by Eq. (5.5).

$$Q = U_{hx} \cdot A_{hx} \cdot T_{m,ln} \quad (5.5)$$

$$T_{m,ln} = \frac{\Delta T_1 - \Delta T_2}{\ln \frac{\Delta T_1}{\Delta T_2}} \quad (5.6)$$

The value of  $T_1$  and  $T_2$ , in the equation above, are evaluated as the difference between the temperature of the hot fluid at the inlet and cold fluid and the outlet, and as the difference between the temperature of the hot fluid at the outlet and the one of cold fluid at the inlet, respectively. Finally, using a value of  $250 \frac{W}{m^2K}$  [48] for the heat exchange coefficient  $U_{hx}$ , the total capital cost for the heat exchangers' network is 42869 \$.

## CHAPTER 6

### CONCLUSIONS

Methanol economy represents a possible solution to meet the environmental targets set by governments. This fuel is a sustainable alternative for fossil-based fuels and chemicals and it can substitute petroleum in all its applications. Methanol is mostly produced in plants that transform syngas into fuel, however an alternative is to use  $\text{CO}_2$  and  $\text{H}_2$  as starting components for the process.

After a brief general introduction on current energy and environmental scenario, the main components used in the plant that produces methanol from  $\text{CO}_2$  have been described. For every part of the process, different solutions have been discussed.

The main focus of the work has been on the creation of the 1D and 2D axisymmetric model of the reactor in which  $\text{CO}_2$  and  $\text{H}_2$  are converted to  $\text{CH}_3\text{OH}$ . In the kinetic model used, only  $\text{CO}_2$  hydrogenation and reverse water-gas shift reactions are considered, and the process is assumed to take place on the catalyst  $\text{CuO}/\text{ZnO}/\text{Al}_2\text{O}_3$ . Both 1D and 2D models involve a set of fully coupled differential equations, which are solved using a non-linear Newton's method.

Because not much experimental data about this process is available, the results of simulations have been validated with data obtained in a reactor that differs from the one for which the kinetic model has been developed. However, using the operation conditions described in the experiment, the data obtained with the mathematical models show trends similar to those reported by Kondarides et al. [45].

After the model validation, a parametric study is performed in order to determine the optimal values of pressure, temperature and composition of the gaseous mixture at the reactor inlet. With the pressure of 5 MPa, inlet temperature of 240°C and composition of 3 H<sub>2</sub>:CO<sub>2</sub>, the selectivity of the catalyst is 81.4 %, while the methanol yield is 30.1 %. From the simulations, the heat extracted from the reactors and the amount of non-reacted gases are determined.

With these data, a thermal integration of the plant has been performed. In this analysis, only the major hot and cold streams have been considered. Then, a plant that uses monoethylamine solution as the absorbent for CO<sub>2</sub> capture, has been compared to a plant that uses a blend of ionic liquid and monoethylamine. Using the blend option, it is possible to meet all the heat demand only through thermal integration. In the future, for a more complete study of the process, a thermo-economic analysis of the overall plant should be performed.

An additional aspect that could be assessed in the future, is how to handle the side products, such as the water produced in the reactor and the oxygen generated in the electrolyzer.

## CITED LITERATURE

1. The Core Writing Team IPCC, R.K. Pachauri, L. Meyer, "Climate Change 2014, Synthesis report", *Intergovernmental Panel on Climate Change*, 2015
2. IEA Website, "Renewables 2020 Data Explorer", <https://www.iea.org/articles/renewables-2020-data-explorer> [Online; accessed 20/02/2021]
3. IEA Website, "Carbon emissions fell across all sectors in 2020 except for one – SUVs", <https://www.iea.org/commentaries/carbon-emissions-fell-across-all-sectors-in-2020-except-for-one-suvs> [Online; accessed 20/02/2021]
4. EU SCIENCE HUB, "Renewable Energy – Recast to 2030 (RED II)", <https://ec.europa.eu/jrc/en/jec/renewable-energy-recast-2030-red-ii>, 2019 [Online; accessed 18/12/2020]
5. Biofuel.org.uk, "History of biofuels", <http://biofuel.org.uk/history-of-biofuels.html> [Online; accessed 12/02/2021]
6. Eurostat: "Wind and water provide most renewable electricity", <https://ec.europa.eu/eurostat/web/products-eurostat-news/-/ddn-20210108-1>, 2020 [Online; accessed 21/02/2021]
7. T. Wilberforce, A.G. Olabi, E. T. Sayed, K. Elsaid, M. A. Abdelkareem, "Progress in carbon capture technologies", *Science of The Total Environment*, Volume 761, 2021.
8. N. Mac Dowell, P. Fennell, N. Shah, et al., "The role of CO<sub>2</sub> capture and utilization in mitigating climate change", *Nature Clim Change* 7, 243–249 (2017)
9. The royal Society, "The potential and limitations of using carbon dioxide", *Policy Briefing*, 2017
10. C. McGlade, "Can CO<sub>2</sub>-EOR really provide carbon-negative oil?", <https://www.iea.org/commentaries/can-co2-eor-really-provide-carbon-negative-oil> [Online; accessed 11/04/2021]

## CITED LITERATURE (continued)

11. G. A. Olah, A. Goepfert, G. K. S. Prakash, "Beyond Oil and Gas: The Methanol Economy", 2006
12. F. Dalena, A. Senatore, A. Marino, A. Gordano, M. Basile, A. Basile, "Methanol, Chapter 1 - Methanol Production and Applications: An Overview", *Elsevier*, 2018
13. Metanex Website, <https://www.methanex.com/about-methanol/how-methanol-made> [Online; accessed 20/03/2021]
14. C. A.S.Hall, J. G.Lambert, S. B.Balogh, "EROI of different fuels and the implications for society", *Energy Policy, Volume 64*, 2014
15. M. Crocker, "Thermochemical conversion of biomass to liquid fuels and chemicals", *Royal Society of Chemistry*, 2010
16. J. S. Srivatsan, M. Amani, "Feasibility Study of Using Excess Heat from GTL Process for Seawater Desalination", *Canadian Center of Science and Education*, 2012
17. H. Purnama, T. Ressler, R.E. Jentoft, H. Soerijanto, R. Schlögl, R. Schomäcker, "CO formation/selectivity for steam reforming of methanol with a commercial CuO/ZnO/Al<sub>2</sub>O<sub>3</sub> catalyst", *Applied Catalysis A: General, Volume 259, Issue 1*, 2004
18. K.M. Vanden Bussche, G.F. Froment, "A steady-state kinetic model for methanol synthesis and the water gas shift reaction on a commercial Cu/ZnO/Al<sub>2</sub>O<sub>3</sub> catalyst", *Journal of catalysis 161*, 1996
19. S. C. Marie-Rose, A. L. Perinet, J.-M. Lavoie, "Conversion of Non-Homogeneous Biomass to Ultraclean Syngas and Catalytic Conversion to Ethanol", *Biofuel's Engineering Process Technology*, 2011
20. F. Robert, "Cost plunges for capturing carbon dioxide from the air", *Science magazine*, 2018
21. D. Kearns, H. Liu, C. Consoli, "Technology readiness and costs of CCS", *Global CCS institute*, 2019
22. IEA (2021): "Zero-emission carbon capture and storage in power plants using higher capture rates", <https://www.iea.org/articles/zero-emission-carbon-capture-and-storage-in-power-plants-using-higher-capture-rates> [Online; accessed 02/03/2021]

## CITED LITERATURE (continued)

23. C. Scholes, "Cling Wrap Captures CO<sub>2</sub>.", , 2010, <https://freshscience.org.au/2010/cling-wrap-captures-co2> [Online; accessed 10/05/2021]
24. M. Santarelli, D. Fino, S. Bensaid, G. Buffo, P. Marocco, F. Salomone, "Studio integrazione di soluzioni innovative per la decarbonizzazione di impianti a combustione, REPORT 1"
25. Office of Energy Efficiency and Renewable Energy, "Hydrogen production: Electrolysis", <https://www.energy.gov/eere/fuelcells/hydrogen-production-electrolysis> [Online; accessed 12/04/2021]
26. I. Goel, "Introduction to Electrolyzer Technologies", <http://www.altenergystocks.com/archives/2021/01/introduction-to-electrolyzer-technologies/>, 2021 [Online; accessed 02/03/2021]
27. S. Shiva Kumar, V. Himabindu, "Hydrogen production by PEM water electrolysis – A review", *Materials Science for Energy Technologies, Volume 2, Issue 3*, 2019
28. K. Chen, D. Dong, S.P. Jiang, "Hydrogen Production from Water and Air Through Solid Oxide Electrolysis", *Production of Hydrogen from Renewable Resources. Biofuels and Biorefineries, vol 5*, 2015
29. IRENA:"Renewable Power Generation Costs in 2019", <https://www.irena.org/publications/2020/Jun/Renewable-Power-Costs-in-2019>, 2020 [Online; accessed 11/04/2021]
30. J. Brauns , T. Turek, "Alkaline Water Electrolysis Powered by Renewable Energy: A Review", *Processes, Vol.8*, 2020
31. S. Mbatha, R. C. Everson, N. M. Musyoka, H. W. Langmi, A. Lanzini, W. Brilmane, "Power-to-methanol process: a review of electrolysis, methanol catalysts, kinetics, reactor designs and modelling, process integration, optimisation, and techno-economics", *Sustainable Energy and Fuels, Issue 14*, 2021
32. H. Nieminen, A. Laari, T. Koiranen, "CO<sub>2</sub> Hydrogenation to Methanol by a Liquid-Phase Process with Alcoholic Solvents: A Techno-Economic Analysis", *Laboratory of Process Systems Engineering*, Lappeenranta-Lahti University of Technology, 2019

## CITED LITERATURE (continued)

33. J. Zhu, S. S. Araya, X. Cui, S. L. Sahlin, S. K. Kær, "Modeling and Design of a Multi-Tubular Packed-Bed Reactor for Methanol Steam Reforming over a Cu/ZnO/Al<sub>2</sub>O<sub>3</sub> Catalyst", *Energies*, 2020
34. S. G. Jadhav, P. D. Vaidya, B. M. Bhanage, J. B. Joshi, "Catalytic Carbon Dioxide Hydrogenation to methanol: A review of recent studies", *Chemical Engineering Research and Design*, Volume 92, Issue 11, 2014
35. J. Ugandhar, K. G. Shankar, D. A. S. Krishna, "A Mini Project Report on Shell and Tube Heat Exchanger", *BC's Thesis MLR Institute of Thecnology*, 2012
36. G. Leonzio, P. U. Foscolo, "Analysis of a 2-D model of a packed bed reactor for methanol production by means of CO<sub>2</sub> hydrogenation", *International Journal of Hydrogen Energy*, Volume 45, Issue 18, 2020,
37. M. Pozzo, A. Lanzini, M. Santarelli, "Enhanced biomass-to-liquid (BTL) conversion process through high temperature co-electrolysis in a solid oxide electrolysis cell (SOEC)", *Fuel*, Volume 145, 2015
38. A. Garg, G. Achari, "A Comprehensive Numerical Model Simulating Gas, Heat, and Moisture Transport in Sanitary Landfills and Methane Oxidation in Final Covers", *Environ Model Assess* 15, 2010
39. J. G. Collier, J. R. Thome, "Convective Boiling and Condensation", *Oxford Science Publications*, 1996
40. D. Schlereth, O. Hinrichsen, "A fixed-bed reactor modeling study on the methanation of CO<sub>2</sub>", *Chemical Engineering Research and Design*, Volume 92, Issue 4, 2014
41. A. Zoughaib, "Energy Integration of Continuous Processes: From Pinch Analysis to Hybrid Exergy/Pinch Analysis", *Elsevier*, 2017
42. W. Roetzela, X. Luob, D. Chenca, "Optimal design of heat exchanger networks", *Computer Aided Chemical Engineering*, Elsevier, Volume 26, 2009
43. COMSOL, "COMSOL Multiphysics Programming Reference Manual, Version 5.5", *COMSOL*, 2019
44. Y. Jaluria, "Computer Methods for Engineering with MATLAB Applications, Second Edition", *CRC Press, Taylor and Francis Group*, 2011

## CITED LITERATURE (continued)

45. M. Kourtelesis, K. Kousi, D. I. Kondarides, "CO<sub>2</sub> Hydrogenation to Methanol over La<sub>2</sub>O<sub>3</sub>-Promoted CuO/ZnO/Al<sub>2</sub>O<sub>3</sub> Catalysts: A Kinetic and Mechanistic Study", *Catalysts*, Vol. 10, 2020
46. E. Heischkamp, M. Varlik, Ö. Korkmaz, G. Oeljeklaus, K. Görner, "Analysis of Operating Conditions of a Flue Gas Scrubbing Process for CO<sub>2</sub> Separation in a Coal-Fired Power Plant", *Energy Procedia*, Elsevier, 2011
47. M. T. Mota-Martinez, P. Brandl, J. P. Hallett, N. Mac Dowell, "Challenges and opportunities for the utilisation of ionic liquids as solvents for CO<sub>2</sub> capture", *Molecular System design and Engineering*, Issue 3, 2018
48. R. Turton, R. C. Bailie, W. B. Whiting, J. A. Shaeiwitz, D. Bhattacharyya, "Analysis, Synthesis, and Design of Chemical Processes", *Prentice Hall*, 2012

## VITA

NAME	Ilaria Tagliaferri
<hr/>	
EDUCATION	
	Bachelor's Degree in Energy Engineering, Jul 2019, Politecnico di Torino, Italy
	Master's Degree in Mechanical Engineering, Aug 2021, University of Illinois at Chicago, USA
	Master's Degree in Energy and Nuclear Engineering, Sep 2021, Politecnico di Torino, Italy
<hr/>	
LANGUAGE SKILLS	
Italian	Native speaker
English	Proficient User
	2019 - IELTS examination (7.5/9)
	A.Y. 2020/2021 One Year of study abroad in Chicago, Illinois
	A.Y. 2019/2021. Lessons and exams attended exclusively in English
Spanish	Independent user
	2018 - language examination B1
	A.Y. 2018/2019 Five Month of study abroad in Barcelona, Spain
<hr/>	
SCHOLARSHIPS	
Fall 2016 - Spring 2019	Italian scholarship for the "Young Talent Project"
Spring 2019	Italian scholarship for the "EU-Young Talent" mobility program in Barcelona, Spain
Fall 2020	Italian scholarship for final project (thesis) at UIC
Fall 2020	Italian scholarship for TOP-UIC students
<hr/>	
TECHNICAL SKILLS	
Average level	Matlab
Average level	Python

**VITA (continued)**

Advanced level      Microsoft Excel

---

**WORK EXPERIENCE AND PROJECTS**

Nov 2018 - June 2019      Bachelor's thesis project: Designed a heat-exchanger for a CSP application, produced the computational model with the software Star-ccm+

Oct 2018 - Jan 2019      Assessment of the efficiency of a simulated building to improve occupants' comfort with the software Polysun

Sep 2020 - Aug 2021      Master's thesis project: A Computational Study of Direct Thermocatalytic Reduction of CO<sub>2</sub> for the Production of Synthetic Methanol

---